

Designing Future Dark Energy Space Missions: I. Building Realistic Galaxy Spectro-Photometric Catalogs and their first applications

S. Jouvel¹, J-P. Kneib¹, O. Ilbert^{3,1}, G. Bernstein², S. Arnouts^{1,4}, T. Dahlen⁵, A. Ealet^{9,1}, B. Milliard¹, H. Aussel⁷, P. Capak⁶, A. Koekemoer⁵, V. Le Brun¹, H. McCracken⁸, M. Salvato⁶, and N. Scoville⁶

¹ Laboratoire d'Astrophysique de Marseille, CNRS-Université d'Aix-Marseille, 38 rue Frederic Joliot-Curie; 13388 Marseille cedex 13, France

² University of Pennsylvania, 4N1 David Rittenhouse Lab 209 S 33rd St Philadelphia, PA 19104, USA

³ Institute of Astronomy, 2680 Woodlawn Drive Honolulu, HI 96822-1897, USA

⁴ CFHT, 65-1238 Mamalahoa Hwy Kamuela, Hawaii 96743 USA

⁵ Space Telescope Science Institute, 3700 San Martin Drive Baltimore, MD 21218 USA

⁶ California Institute of Technology 1200 East California Blvd. Pasadena CA 91125, USA

⁷ Service d'Astrophysique, CEA-Saclay, 91191 Gif-sur-Yvette, France

⁸ Institut d'Astrophysique de Paris 98bis, bd Arago F75014 Paris, France

⁹ Centre de Physique des Particules de Marseille, 163, avenue de Luminy, Case 902, 13288 Marseille cedex 09, France

DRAFT VERSION: OCTOBER 29, 2018

ABSTRACT

Context. Future dark energy space missions such as JDEM and EUCLID are being designed to survey the galaxy population to trace the geometry of the universe and the growth of structure, which both depend on the cosmological model. To reach the goal of high precision cosmology they need to evaluate the capabilities of different instrument designs based on realistic mock catalogs of the galaxy distribution.

Aims. The aim of this paper is to construct realistic and flexible mock catalogs based on our knowledge of galaxy populations from current deep surveys. We explore two categories of mock catalogs : (i) based on luminosity functions that we fit to observations (GOODS, UDF, COSMOS, VVDS) (ii) based on the observed COSMOS galaxy distribution.

Methods. The COSMOS mock catalog benefits from all the properties of the data-rich COSMOS survey and the highly accurate photometric redshift distribution based on 30-band photometry. Nevertheless this catalog is limited by the depth of the COSMOS survey. Thus, we also evaluate a mock galaxy catalog generated from luminosity functions using the *Le Phare* software. For these two catalogs, we have produced simulated number counts in several bands, color diagrams and redshift distributions for validation against real observational data.

Results. Using these mock catalogs we derive some basic requirements to help design future Dark Energy missions in terms of the number of galaxies available for the weak-lensing analysis as a function of the PSF size and depth of the survey. We also compute the spectroscopic success rate for future spectroscopic redshift surveys (i) aiming at measuring BAO in the case of the wide field spectroscopic redshift survey, and (ii) for the photometric redshift calibration survey which is required to achieve weak lensing tomography with great accuracy. In particular, we demonstrate that for the photometric redshift calibration, using only NIR (1-1.7 μ m) spectroscopy, we cannot achieve a complete spectroscopic survey down to the limit of the photometric survey ($I < 25.5$). Extending the wavelength coverage of the spectroscopic survey to cover 0.6-1.7 μ m will then improve the fraction of very secure spectroscopic redshifts to nearly 80% of the galaxies, making possible a very accurate photometric redshift calibration.

Conclusions. We have produced two realistic mock galaxy catalogs that can be used in determining the best survey strategy for future dark-energy missions in terms of photometric redshift accuracy and spectroscopic redshift surveys yield. *These catalogues are publicly accessible at <http://lamwww.oamp.fr/cosmowiki/RealisticSpectroPhotCat>, or by request to the first author of this paper.*

Key words. redshift – JDEM – cosmology – surveys – mock catalog

1. Introduction

The prospect for high-precision cosmological inferences from large galaxy surveys has prompted the initiation of several projects with the goal of surveying thousands of square degrees of sky in multiple filters with or without spectroscopy. The ground based projects [e.g. current KIDS, DES, and future Pan-STARRS, LSST in imaging and current SDSS-III/BOSS and future WFMOS BigBOSS in spectroscopy], and the space based missions [JDEM, and EUCLID, or their former and fu-

ture concepts] all propose to conduct wide field galaxy survey (in imaging with or without spectroscopy) in order to exploit the power of weak gravitational lensing [WL] and galaxy clustering (using baryonic acoustic oscillations [BAO] with or without redshift distortion measurements [RD]) to elucidate the cause of the acceleration of the Hubble expansion (Riess et al. (1998), Perlmutter et al. (1999), Astier et al. (2006), Kilbinger et al. (2009)). Proper design and forecasting of the performance of these experiments require an accurate estimate of the “yield” of galaxies, such as number counts, redshift sizes and color distributions, from a chosen survey configuration. It is typically straightforward to estimate the expected resolution and noise properties of the telescope and instrument, but more

difficult to quantify the number and properties of the “useful” galaxies available on the sky. A good forecast requires that we estimate the density of galaxies on the sky over the joint distribution of:

(i) redshift; (ii) angular size, expressed as half-light radius $r_{1/2}$; (iii) apparent magnitudes and colors in any chosen instrument passbands; (iv) emission-line strengths.

The first three properties are essential to knowing whether a given galaxy will be detected at sufficient signal-to-noise (S/N) and resolution to determine its shape and its photometric redshift. The last property, the emission-line strength, is essential to estimating the depth and completeness that any spectroscopic redshift survey will achieve. Spectroscopic redshift accuracy is needed to conduct the best possible BAO/RD measurements, and to calibrate photometric redshift (“photo- z ”) estimators that are essential for WL tomographic measurement (e.g. Massey et al. (2007)).

In this paper we present two simulated catalogs of galaxy properties based on current deep surveys that we will use in forthcoming papers (Jouvel et al. 2009 in prep.) to forecast the performance of WL Dark Energy space based missions. Unfortunately we cannot simply use a catalog from some completed survey, since (1) no single survey of useful depth has simultaneously observed all of the listed properties for its target galaxies, and (2) the proposed surveys will exceed the depth, field of view, resolution, with or without wavelength coverage of most existing observed galaxy catalogs. For example, the space based spectroscopic survey will likely mainly be conducted in the near-infrared, surpassing any current infrared spectroscopic redshift survey. The mission concepts of SNAP, Destiny, and EUCLID propose near-infrared (NIR) imaging over very wide areas, but only a few square arcminutes of HST/NICMOS imaging data with the UDF (Coe et al. 2006) and close to one degree down to $K \sim 23$ for ground based data with the UKIDSS survey on the UKIRT telescope (Lawrence et al. 2007) are available to date at these magnitude levels, insufficient to serve as a robust source model. Any relevant simulated catalogs must therefore include some degree of extrapolation or modelling of the source population.

In this paper, we explain how we have constructed 2 simulated galaxy catalog based on deep survey data. Section 2 explain the methodology used. In section 3 we validate these simulated catalogs by comparing their predicted magnitude, color, redshift, size, and emission-line strength distributions to real survey data taking into account the survey selection functions.

Although this work was initiated in the context of the SNAP collaboration (see our first results in Dahlen et al. (2008)), it can easily be adapted to any instrument concept for a proper evaluation of its merit. When necessary we assume a Λ CDM universe: $(\Omega_M, \Omega_\Lambda) = (0.3, 0.7)$ and $H_0 = 70$ km/s/Mpc. All magnitudes used in this paper are on the AB system.

2. Realistic mock Galaxy Catalog

For both of our simulated catalogs, each galaxy is assigned a spectral energy distribution (SED), which can be integrated over any instrumental passband to forecast an apparent magnitude. Our first fully simulated catalog has been generated by using “Le Phare” simulation tool¹ (Arnouts and Ilbert 2009 in prep) with an analytic luminosity function based on the GOODS survey from the work of Dahlen et al. (2005). We will refer to our

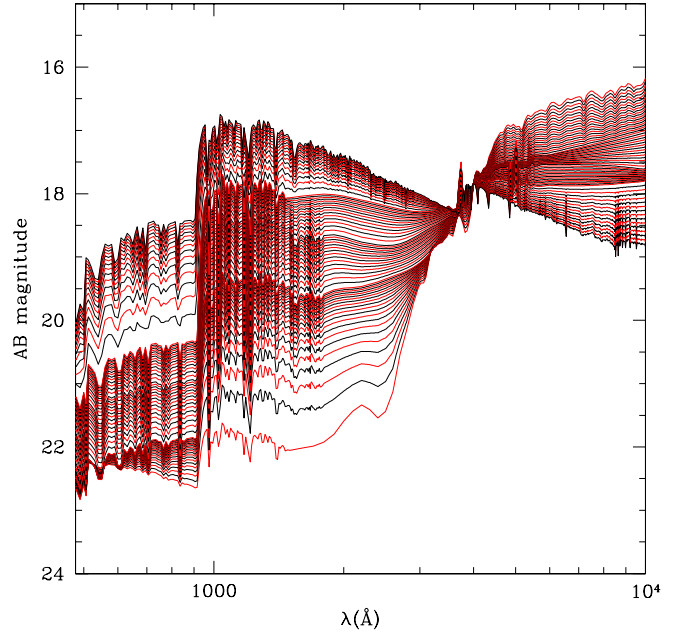


Fig. 1. Extended CWW library of SED templates. This represents the full range of SED template linearly interpolated between the 4 CWW templates and one star-forming template in AB magnitude (arbitrarily flux scaled at 4000\AA).

derived simulated catalog as the *GOODS Luminosity Function Catalog (GLFC)*.

2.1. GLFC - GOODS Luminosity Function based Catalog

2.1.1. SED Library

The GLFC relies on two ingredients :

- A set of SEDs spanning the entire range from Elliptical to starbursting galaxy,
- A redshift evolving luminosity function (LF) per type.

Those ingredients are the basic requirements to generate a catalog that can predict global distributions such as magnitude, redshift and color counts. We use the Coleman Extended library (CE) for our templates of galaxies. This list is based on the four observed spectra of Coleman et al. (1980) corresponding to an Elliptical, Sbc, Scd and Irregular, which have been extrapolated in the UV and IR wavelengths domain by using synthetic spectra from the GISSEL library (Charlot and Bruzual, 1996). To reproduce observed colors bluer than the CE templates, we add one spectrum of star-forming galaxies computed with the GISSEL model for solar metallicity, Salpeter IMF, constant star formation rate and 0.05 Gyr age. Following the approach adopted by Sawicki et al. (1996), we have linearly interpolated the original 5 SEDs to provide a finer grid of spectral-type coverage with a total library of 66 templates shown in **Figure 1**. In **Figure 2**, we draw magnitudes of the 5 main templates in a magnitude-wavelength plane by bins of redshifts in order to show colors of these templates that may help in deciding which sensitivities are needed to detect galaxies inside different passbands.

¹ Arnouts http://www.oamp.fr/people/arnouts/LE_PHARE.html

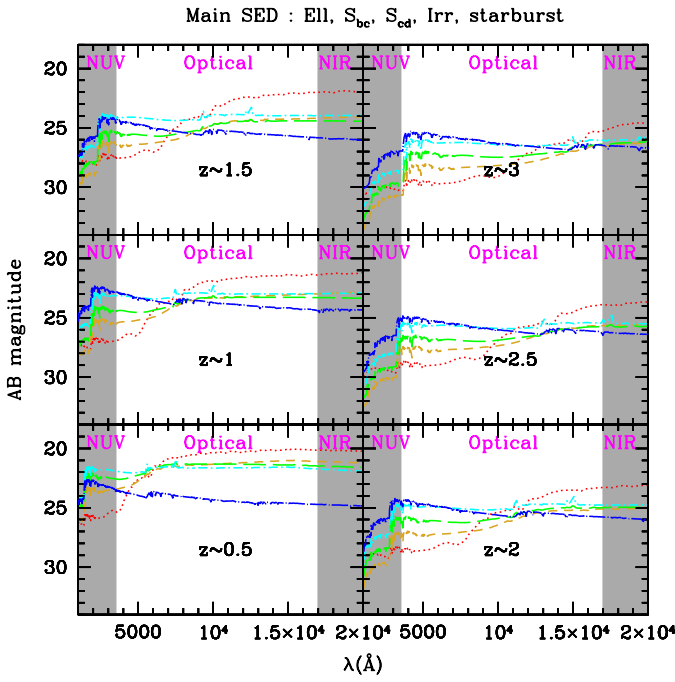


Fig. 2. Magnitudes of the 5 main templates composed by the 4 CWW : *Ell* (red dotted), *S_{bc}* (gold dashed), *S_{cd}* (green long-dashed), *Irr* (cyan dot-dashed) and one star-forming (blue long dot-dashed) shown at some given redshift of 0.5,1,1.5,2,2.5,3. The templates are M^* galaxies as given in Table 2.

Table 1. Restframe colors of SED templates.

LF	E(B-V)	types	$B - V(\text{restframe})$
1	0	1 → 17	1.069 → 0.701
2	0	17 → 55	0.701 → 0.2167
3	0	55 → 66	0.2167 → -0.0301
3	0.1	56 → 66	0.3252 → 0.1016
3	0.2	56 → 66	0.4592 → 0.2345
3	0.3	56 → 66	0.5945 → 0.3686
Main templates	E(B-V)	nbr	$B - V(\text{restframe})$
<i>Ell</i>	0	1	1.069
<i>S_{bc}</i>	0	21	0.6262
<i>S_{cd}</i>	0	36	0.5077
<i>Irr</i>	0	51	0.3185
<i>star-forming</i>	0	66	-0.0301

2.1.2. Extinction

We have diversified our templates by adding extinction computed from the Calzetti extinction law (Calzetti et al. 2000) with the excess reddenning values $E(B - V)$ of 0,0.1,0.2,0.3 mag and using the extinction formula:

$$flux_{attenuated}(\lambda) = flux_{intrinsic}(\lambda) \cdot 10^{-0.4 * k(\lambda) \cdot E(B-V)} \quad (1)$$

The $k(\lambda)$ values follow the Calzetti law. Each $E(B - V)$ value will be applied to the irregular and star-forming templates, increasing the number of templates for those types. Finally we also include the Lyman absorption by the Intergalactic Medium as a function of redshift, following Madau (1995).

2.1.3. GLFC Luminosity Function

The GLFC is generated by assuming a luminosity function (LF) for galaxies of 3 different types, then drawing galaxies from these LFs to populate our simulated sky area. We have selected these 3 types following the B-V rest-frame colors given in Dahlen et al. (2005) (see table 1). We start with the LF estimated in rest-frame B band by Dahlen et al. (2005) in the 3 spectral types inside 4 redshifts bins over $0 < z < 1$. Dahlen et al. (2005) derive these LFs by fitting to photo-z data from the GOODS survey. We have extrapolated these LFs to $z = 6$ to be complete for the galaxies likely to be used in future surveys. The Dahlen $z = 1$ LF for each type is held nearly fixed for $1 < z < 6$, with some adjustments made to improve the match to data from the COSMOS survey (described below).

Table 2 gives the LF calculated for 3 galaxy types extrapolated until redshift $z \simeq 6$ as explained above. To produce the mock catalog, knowing the luminosity function, Le Phare derives a number of objects by magnitude and redshift bins (z, m) using a Schechter function (Schechter 1976) :

$$n(M(z, m))dM = \phi^* \left(\frac{M(z, m)}{M^*} \right)^\alpha \exp \left(- \frac{M(z, m)}{M^*} \right) \frac{dM}{M^*} \quad (2)$$

M is the absolute magnitude which is a function of redshift and apparent magnitude (z, m) , M^* , ϕ^* and α are the parameters of the Schechter function given in the Table 2.

According to the adopted area, the simulated galaxy counts in each magnitude-redshift-type bin are drawn from a Poisson distribution of the expected number based on the LF.

Note that the luminosity function parameters depend on the cosmological model assumed (as the luminosity function is expressed in physical units). However the resulting galaxy catalog can be considered to be independent of the input cosmological parameters assumed here, as it is built to reproduce the *observed* galaxy distribution and properties.

Table 2. Luminosity Function in the B band extrapolated to match COSMOS colors and number counts used to create the GLFC catalog.

LF	z	ϕ^*	M^*	α
1	0.5	16.7e-4	-21.15	-0.71
1	0.75	18e-4	-21.13	-0.50
1	1.0	9.5e-4	-21.72	-0.98
1	2.0	8.5e-4	-21.72	-0.98
1	3.0	7.5e-4	-21.72	-0.98
1	6.0	6.5e-4	-21.72	-0.98
2	0.5	24.0e-4	-21.08	-1.37
2	0.75	25.0e-4	-21.29	-1.17
2	1.0	25.0e-4	-21.2	-1.1
2	1.5	24.4e-4	-21.15	-0.05
2	2.0	24.4e-4	-21.15	-0.99
2	3.0	24.4e-4	-21.15	-0.99
2	6.0	24.4e-4	-21.15	-0.85
3	0.5	48.6e-4	-18.84	-1.1
3	0.75	33.1e-4	-19.67	-1.18
3	1.0	33.1e-4	-20.55	-1.52
3	1.5	30.0e-4	-20.62	-1.62
3	2.0	25.0e-4	-20.72	-1.7
3	3.0	25.0e-4	-20.72	-1.8
3	6.0	25.0e-4	-20.72	-1.8

Drawing from the luminosity functions gives the galaxy distribution over the joint magnitude-color-redshift space. We assign a half-light radius to each galaxy as follows: we first calculate the galaxy's apparent magnitude in the F814W HST filter. Leauthaud et al. (2007) provides a size-magnitude catalog for the 1.64 deg² COSMOS survey executed in this filter. We assign the simulated galaxy a half-light radius that is drawn at random from all galaxies of the same F814W apparent magnitude in the observed COSMOS catalog. Thus the size-magnitude distribution of the simulated catalog will, by construction, exactly match the COSMOS observations. The procedure does not reproduce any additional dependence of galaxy size upon type, color, or redshift using the COSMOS catalog. Any further correlation between size and other parameters such as color, redshift and galaxy type could in principle be implemented by following the COSMOS catalogue. As this is not needed in this paper, we have not implemented these higher order correlations. However the size-magnitude relation of the mock catalogue do follow the COSMOS relation.

2.1.4. Photometric Noise

A real survey has noise from the finite photon counts and detector noise. Estimation of this noise is of course essential for forecasting survey performance. It may also be important for validation of the simulation against real data, since the noise can induce biases on number counts. Le Phare produces both noiseless magnitudes and noisy magnitudes for each chosen observation bandpass. The noisy magnitudes are randomly drawn from a Gaussian distribution with mean and standard deviation (m, err_m). We define a reference couple (m^*, err^*). At magnitude $m < m^*$, the object noise is dominant and we assume that the magnitude error follows a power law of the adjustable form :

$$err_m = 10^{(0.4(p+1)(m-m^*))} \quad (3)$$

At magnitude $m > m^*$, the sky noise is dominant and we assume the error on magnitude follows an exponential law :

$$err_m = err^* / 2.72 \cdot \exp(10^{(q(m-m^*))}) \quad (4)$$

(p, q) are the slopes for the power laws, both derived from the survey characteristics.

We will, however, use noiseless magnitudes for the validation tests in this paper, because the comparison surveys (*e.g.* the UDF) have high S/N in the regimes of comparison, and because the noise-induced biases are generally small.

2.2. CMC - The COSMOS Mock Catalog

The second simulated galaxy catalog is built directly from the observed COSMOS catalog of Capak et al. (2009) in prep. and Ilbert et al. (2009). We will refer to this simulation as the COSMOS Mock Catalog (CMC).

2.2.1. The COSMOS catalog

The COSMOS photometric-redshift catalog (Ilbert et al. 2009) was computed with 30 bands over ~ 2 -deg² taken from GALEX for UV bands, Subaru for the optical (U to z), and CFHT, UKIRT and Spitzer for the NIR bands. However, we restrict our mock catalog to the central square area of 1.38 deg² which is fully covered by HST/ACS imaging. The COSMOS-ACS catalog gives 592000 galaxies for an area of 1.38deg². This is roughly a density of 120 galaxies per arcmin² down to $i^+ < 26.5$. In the

COSMOS photometric-redshift catalog, 10% of this surface corresponds to areas masked because of bright stars that prevent quality multiband photometry in the extended bright star halos. The effective area is thus in fact 1.24 deg² of unmasked region with a total number of 538000 simulated galaxies out to $i^+ < 26.5$ leading again to roughly a density of 120 gal/arcmin². Point sources such as stars and X ray sources (mostly dominated by an AGN) were also removed from the mock catalog.

The photo-z accuracy is based on a comparison to spectroscopic surveys like the zCOSMOS (bright survey down to $i_{med}^+ < 22.5$ with 4148 galaxies and faint down to $i_{med}^+ < 24$ with 148 galaxies) and also the MIPS infrared selected sample (bright and faint with 317 galaxies, Figure 7 and 8 of Ilbert et al. (2009)). The COSMOS photo-z accuracy is $\sigma_{\Delta z/(1+z_s)} = 0.007$ at $i^+ < 22.5$ with a catastrophic rate below 1% (see Figure 6 of Ilbert et al. (2009)). At fainter magnitudes and $z < 1.25$, the estimated accuracy is $\sigma_{\Delta z} = 0.02, 0.04, 0.07$ at $i^+ \sim 24, i^+ \sim 25, i^+ \sim 25.5$, respectively. The accuracy is degraded at $i^+ > 25.5$. The deep NIR and IRAC coverage enables the photo-z to be extended to $z \sim 2$ albeit with a lower accuracy ($\sigma_{\Delta z/(1+z_s)} = 0.06$ at $i_{AB}^+ \sim 24$) (see Ilbert et al. (2009) for more details).

Despite the lower photo-z accuracy at $i^+ > 25.5$ and $z > 1.25$ and the possible bias due to the faint AGN contribution, we use the full COSMOS catalog. Indeed, the photo-z accuracy is not crucial for the simulation. The COSMOS catalog is only used to obtain a representative population of galaxies in term of density and mix of galaxy types. Since the predicted apparent magnitudes are calculated from the best-fit templates, the photo-z accuracy has no impact on our ability to link the simulated redshift to the predicted colors. The only risk of including lower quality photo-z's is to degrade slightly the catalog representativity, possibly biasing the redshift distribution at $z > 1.25$.

2.2.2. The mock catalog construction

The principle of our simulation is to convert the observed properties of each COSMOS galaxy into simulated properties that can then be viewed using any possible instrument configuration. A photo-z and a best-fit template (including possible additional extinction) are associated with each galaxy of the COSMOS catalog.

The first step is to integrate the best-fit template (in the observer frame) through the instrument filter transmission curves to produce simulated magnitudes in the instrument filter set.

The second step is to apply random errors to the simulated magnitudes, based on the magnitude-error relations established in each filter (see Section 2.1.4).

Importantly, all the COSMOS measured properties are propagated to the simulated galaxies, for instance, the galaxy half-light radius as measured on the ACS images by Leauthaud et al. (2007).

This approach presents the following advantages:

- the simulated mix of galaxy populations is, by construction, representative of a real galaxy survey,
- additional quantities measured in COSMOS (like the galaxy size, UV luminosity, morphology, stellar masses, correlation in position) can be easily propagated to the simulated catalog.

The COSMOS mock catalog is limited to the range of magnitude space where the COSMOS imaging is complete ($i_{AB}^+ \sim 26.2$ for a 5σ detection, see Capak et al. (2007) and Capak et al. (2009) in prep.

2.2.3. Simulating emission lines

For each galaxy of the COSMOS mock catalog we have associated emission line fluxes. This feature is useful to predict the size and the depth of a spectroscopic redshift sample. We modeled the emission line fluxes ($\text{Ly}\alpha$, [OII], $\text{H}\beta$, [OIII] and $\text{H}\alpha$) of each galaxy as explained below.

We used the method described in Section 3.2 of Ilbert et al. (2009). Using the Kennicutt (1998) calibration, we first estimated the star formation rate (SFR) from the dust-corrected UV rest-frame luminosity already measured for each COSMOS galaxy. The SFR can then be translated to an [OII] emission line flux using another calibration from Kennicutt (1998). We checked that the relation found between the [OII] fluxes and the UV luminosity is in good agreement with the VVDS data (see Fig.3 of Ilbert et al. (2009)) and still valid for different galaxy populations. For the other emission lines, we adopted intrinsic, unextincted flux ratios of $[\text{OIII}]/[\text{OII}] = 0.36$; $\text{H}\beta/[\text{OII}] = 0.28$; $\text{H}\alpha/[\text{OII}] = 1.77$ and $\text{Ly}\alpha/[\text{OII}] = 2$ (McCall et al. (1985), Moustakas et al. (2006), Mouhcine et al. (2005), Kennicutt (1998)). The approach of determining the $\text{Ly}\alpha$ line flux through its ratio with the OII emission line flux is perhaps not good, but since the $\text{Ly}\alpha$ line becomes visible to optical-NIR wavelength surveys only beyond $z \sim 3$, it will not have a big impact. Finally, we reduce each galaxy's line flux using the best-fit dust attenuation found with the template fitting procedure in the COSMOS photo-z catalog.

The same procedure can be applied to the GLFC since we can calculate the UV absolute luminosity the same way as for the CMC.

The COSMOS mock Catalog (CMC) has the advantage over the GLFC that it better preserves the relations between galaxy size and color (and presumably type and redshift). The CMC may also reproduce color distributions more accurately, since the population has not been reduced to three galaxy types as in the GLFC. The CMC is, however, limited by construction to the range of magnitude space where the COSMOS imaging is complete, whereas the GLFC can be extrapolated to fainter galaxies. Our validation tests below will compare the differences of these two simulation approaches. It is important to stress that all the following galaxy number densities correspond to mask-corrected areas. Hence for real surveys, those numbers would have to be reduced by a factor of $\approx 10\%$ as observed in COSMOS field.

3. Validation

The aim of these mock catalogs is to predict the performance of future surveys such as JDEM and EUCLID. The depth of the foreseen surveys may be significantly fainter than the deepest existing spectroscopic and NIR imaging wide field surveys, so a comprehensive observational validation of the catalog is not yet possible—especially in terms of NIR photometry and redshift distribution. We should, however, prove that the GLFC and CMC are consistent with existing data. For this validation, we will compare the galaxy counts, color distributions, redshift distributions, and emission-line distributions to a selection of the deepest available relevant survey data. The comparison data are taken from:

- The HST Ultra-Deep Field (UDF) catalog (Coe et al. 2006)² and included references covers 11.97 arcmin^2 in the 4

HST/ACS filters F435W, F606W, F775W and F850LP, referred to as B , V , i , and z bands, respectively, and 5.76 arcmin^2 for the NICMOS filters F110W and F160W, referred to as J and H bands. The UDF detects objects are at 10σ for $z < 28.43$, $i < 29.01$ and $J < 28.3$, significantly fainter than the expected depth of any of the aforementioned proposed surveys. Due to the small area, the UDF is more sensitive to the cosmic variance, but it is useful for comparisons at faint magnitudes.

- The GOODS (Great Observatories Origins Deep surveys) v1.1 survey catalog³ (Giavalisco et al. 2004). The GOODS observations are split into northern and southern fields. Each field covers 160 arcmin^2 in the same $BViz$ filters as the UDF, and is 90% complete at $z \approx 26$.
- The GOODS-MUSIC (MULTIwavelength Southern Infrared Catalog) sample (Grazian et al. 2006) has been constructed with public data of the GOODS-S field, NIR Spitzer data from IRAC instrument (3.6, 4.5, 5.8 and $8.0 \mu\text{m}$) and U-band data from the 2.2ESO and VLT-VIMOS covering 140 arcmin^2 . This catalog is both z and K_s -selected and is 90% complete for $K_s < 23.8$ and $z < 26$.
- The VVDS-DEEP first epoch public release⁴ includes photometric data in BVRI VIRMOS-VLT bands over 0.49 deg^2 (McCracken et al. 2003); a spectroscopic survey of targets with $I_{AB} < 24$ (Le Fèvre et al. 2005) with a sampling rate of 0.2 and a mean redshift of 0.86.
- The VVDS-DEEP NIR J and K_s photometry (Iovino et al. 2005) covers 170 arcmin^2 and is complete for $K_s < 22.5$. This sample contains the $BVri$ VIRMOS-VLT band and the JKs ESO/NTT (New Technology Telescope) using the SOFI Near Infrared imaging camera.

A cut in the size-magnitude plane is applied to each dataset in order to remove stellar contamination, in case this has not already been done for published catalogs.

For each of the above listed surveys, both a CMC and a GLFC are constructed as described above, projecting both mock catalogs onto the real surveys' filter sets.

3.1. Galaxy Counts

We compare the simulated galaxy counts (dN/dm) to those in the real catalogs listed above. The SED of each simulated galaxy is integrated over the bandpass of each real catalog.

In **Figure 3** we compare the differential galaxy counts in the B , V , i , and z bands of the UDF and GOODS to those synthesized from the GLFC and CMC simulations. The blue solid line is the COSMOS mock catalog (CMC) and the black dot-dashed line is the *Le Phare simulation* based on the GOODS LF (GLFC). The real observations are: the UDF (red dotted); GOODS North (long-dashed green) and South (dashed magenta). The UDF counts in the NIR are also compared to the simulations. An excellent agreement is seen between all sources for $21 < m < 26$, where each is complete, with some tendency for the UDF counts to be lower than other surveys. We attribute this to cosmic variance because of the very small UDF survey area. The difference between the simulated catalogs and the GOODS South is generally less than the difference between GOODS North and South ($\approx 15\%$). Note that the CMC becomes incomplete for $m > 26$ ($m > 25$ in the $1.6 \mu\text{m}$ band), so will underestimate the galaxy yield in surveys deeper than these limits.

³ <http://archive.stsci.edu/prepds/goods/>

⁴ <http://cencos.oamp.fr/>

² <http://adcam.pha.jhu.edu/~coe/UDF/>

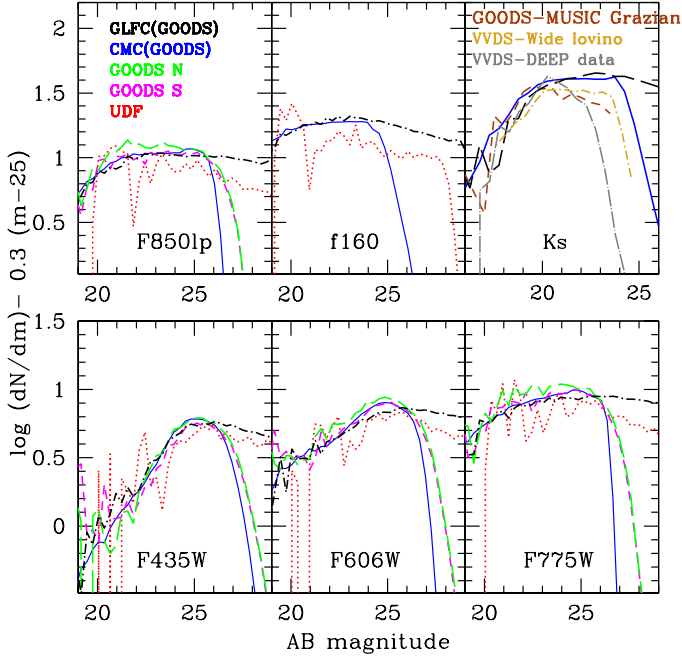


Fig. 3. Differential galaxy counts for F435W (B band), F775W (i band), F850LP (z band), F160W (H band) and the K_s band comparing mock catalogs to real observations of UDF and GOODS surveys.

We also compare in Figure 3, the simulated K_s band counts to the GOODS-MUSIC and VVDS data. The K_s -band VVDS data of Iovino et al. (2005) are 90% complete at $I_{AB} = 25.5$. We see a very good agreement between the VVDS, GOODS-MUSIC and simulated catalogs at $K_s < 20$ and some discrepancies at fainter magnitudes. However, we measure a mean less than 17.9% difference between VVDS Iovino and CMC, 14.4% difference between VVDS Iovino and GLFC and 17.4% between GOODS-MUSIC and VVDS Iovino within the observation limits of these 2 surveys. We conclude that both simulated catalogs are well reproducing the K_s counts.

3.2. Colors

Figure 4 compares the $B - z$ color distribution of the simulated catalogs to those of GOODS and UDF galaxies. The blue solid line is the COSMOS catalog (CMC) and the black dotted line is the GLFC catalog in GOODS filters. The real observations are: the UDF (dot-dashed red); GOODS North (long-dashed green) and South (dashed magenta). The indicated cut in S/N and magnitude are applied to F850LP (z Band) for each catalog. The magnitude cuts in the B and z bands are taken following the COSMOS completeness in each of these bands. There is a good agreement in these optical wavelengths. The simulated catalogs have median and mean $B - z$ colors in agreement at a few percent with the UDF and GOODS catalogs (see **Table 3**).

The UDF seems relatively deficient in the reddest galaxies, again perhaps a manifestation of cosmic variance, which is most severe for the highly-clustered red-sequence galaxies. This is an expected result and is not an issue with the catalogues since the UDF may be under-dense due to its small survey area.

Figure 5 compares simulated $B - K_s$ colors to those in the GOODS-MUSIC and VVDS-DEEP catalog. The blue solid line is the COSMOS mock catalog (CMC) and the black dotted line

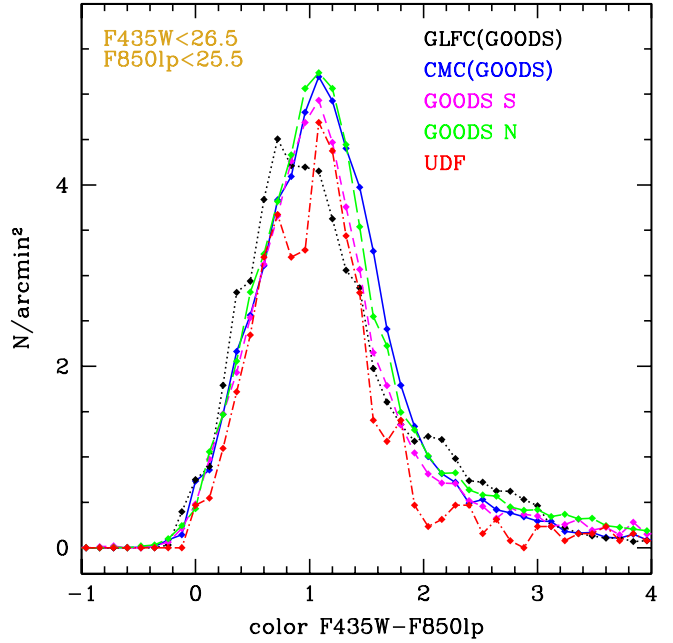


Fig. 4. Color histogram of F435W (B Band)-F850lp (z Band) comparing mock catalogs to real observation of UDF and GOODS surveys.

Table 3. Mean and median of the $B - z$ color distributions with the magnitude cuts of **Figure 4** corresponding to the completeness of the CMC.

Catalogs	Mean	Median	survey area	mag limit
CMC(GOODS)	1.24	1.14	1.24 deg ²	$I \sim 26$
GLFC(GOODS)	1.2	1.05	0.1 deg ²	$R \sim 31$
GOODS-S	1.26	1.1	160 arcmin ²	$z \sim 26$
GOODS-N	1.3	1.13	160 arcmin ²	$z \sim 26$
UDF	1.16	1.06	11.97 arcmin ²	$z \sim 28.43$

is the GLFC catalog. The observational data are the GOODS-MUSIC survey (top panel in dashed magenta) and VVDS-DEEP survey (bottom panel in dashed green). We choose to cut at 22.5 AB mag in the K_s Band due to the VVDS incompleteness and the variability of the GOODS-MUSIC survey area beyond this magnitude. The color distributions in NIR agree well inside the completeness limits imposed by the different surveys, the CMC $z < 25.5$ and $B < 26.5$ and the GOODS-MUSIC survey $K_s < 22.5$. The GOODS-MUSIC data have lower B - K_s counts which is explained by the number count difference at $K_s > 20$ in the K_s -band between both simulated catalogs and the Grazian counts (see Figure 3). However, the mean and median colors are in good agreement. The agreement is much better when comparing our mock catalogs to the VVDS-DEEP survey (bottom panel of Figure 5).

3.3. Redshifts

Comparison of the simulated redshift distributions to real data is likely less accurate than colors or magnitudes, since real redshift surveys are much shallower and have significant incompleteness. Nonetheless, **Figure 6** shows median and quartiles of the redshift distributions vs I -band magnitude of the CMC (blue

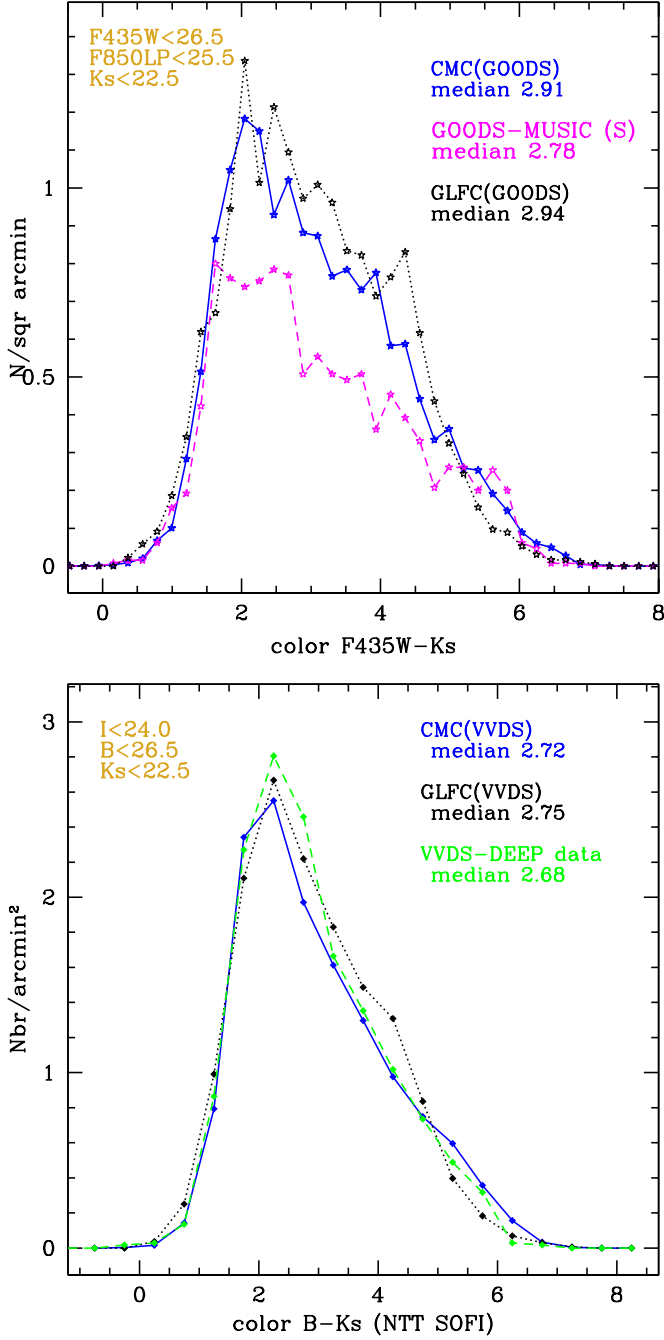


Fig. 5. Color histogram of F435W (B Band)-Ks comparing mock catalogs to real observation of GOODS and VVDS-DEEP surveys.

medium-thickness line) and the GLFC catalogs (black thin line) in the VVDS filters compared to the VVDS-DEEP redshift distribution (green high-thick line). The dotted lines represents the quartiles and solid lines the median of the redshift distribution.

The redshift quartiles of the CMC agree very well with the VVDS spectroscopic redshift distribution to the $I = 24$ limit of the latter. The GLFC seems to have a lower median redshift, probably due to the GOODS LF used to produce the catalog. The mean difference of the median redshift is 0.02 and 0.07 for the CMC and GLFC catalogs, respectively. We conclude not surprisingly that the CMC is probably a better representation of

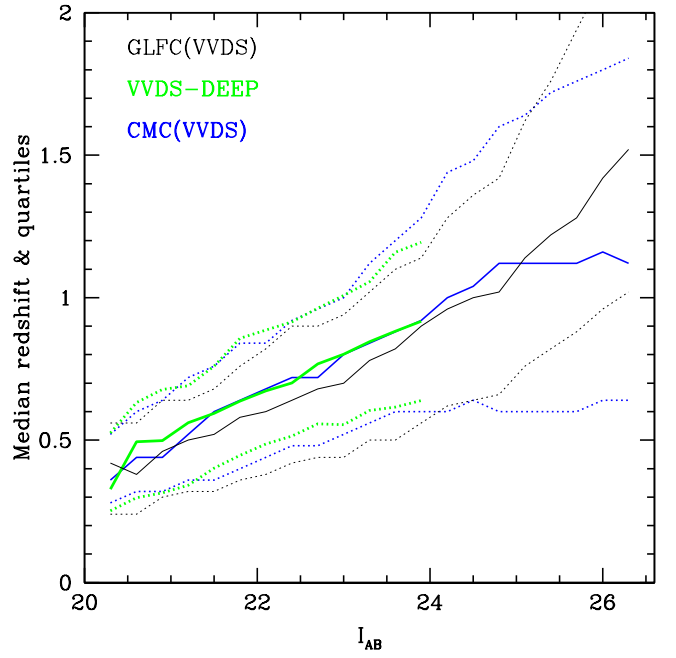


Fig. 6. Redshift distribution as a function of the VVDS i band magnitude compared to mock catalogs redshift distribution.

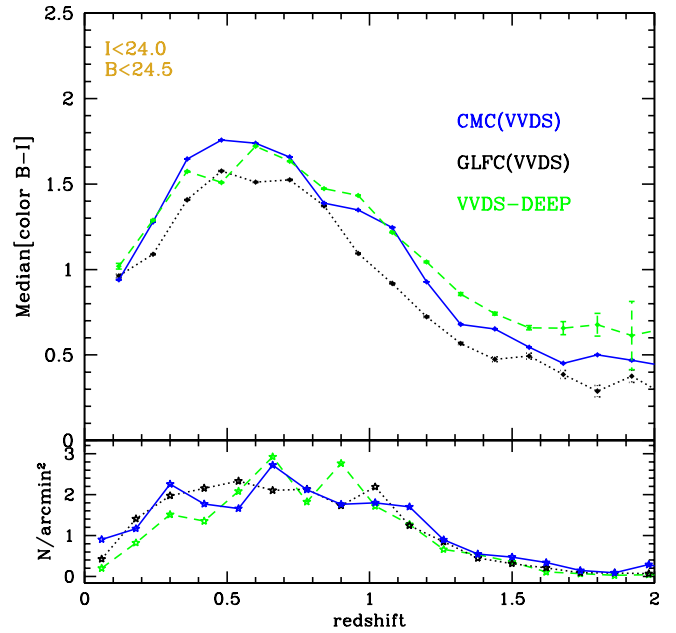


Fig. 7. Median of $B-i$ color (VVDS bands) as a function of redshift for GLFC and CMC mock catalogs and the VVDS-DEEP survey.

the magnitude-redshift distribution, and is as accurate as current data can validate.

Figure 7 plots median $B-i$ color vs redshift for the simulated catalogs CMC (blue solid line) and GLFC (black dotted line) in the VVDS passbands compared to the VVDS-DEEP survey (green dashed line). All catalogs have been restricted to $I < 24$, the completeness domain of the VVDS-DEEP redshift survey. The colors agree to 0.1–0.2 mag until $z \sim 2$. Above this redshift

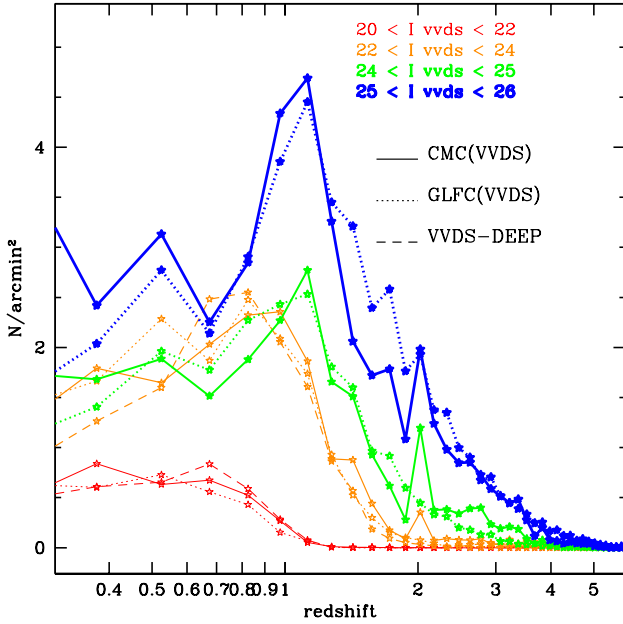


Fig. 8. Redshift distribution of the VVDS-DEEP survey, the COSMOS survey and the GLFC catalog from the GOODS luminosity function.

the VVDS survey is likely to be highly incomplete, even for blue galaxies, as no strong emission lines are available in the VVDS spectral wavelength range and due to the $I = 24$ magnitude cut (see Figure 6) for the median redshift and quartiles of the distribution.

We compare the redshift distributions (Figure 8) for different magnitude cuts (different colors and thickness). There is a very good agreement between the VVDS-DEEP (dashed lines), the COSMOS survey (solid lines) and the GLFC (dotted lines) redshift distributions.

The CMC and the VVDS-DEEP catalog show very good agreement. This figure shows that both mock catalogs are well reproducing the number density inside the VVDS volume : ($0 < z < 1.5$ and $I < 24$) and agree at higher magnitude and redshift. The GLFC is based on the GOODS luminosity function ((Dahlen et al. 2005)) which has equivalent depth to the VVDS galaxy sample. However when looking at Figure 6, the VVDS magnitude-redshift distribution seems to be in better agreement with the CMC than the GLFC.

3.4. Emission-Line Strength

Future dark energy surveys need large spectroscopic redshift samples for calibrating photometric redshifts, measuring accurately the BAO, and for other probes using spectroscopic samples of galaxies. Thus it is crucial to have realistic emission lines allowing predictions of the success rate, depth, and size of spectroscopic samples that we will need. Although, the CMC does not reproduce absorption lines, it simulates emission lines for all galaxies in the catalogue, which allows a first estimation of spectroscopic survey capabilities. The validation of the emission line strength can be found in Figure 3 of Ilbert et al. (2009). This

figure shows the relation between the OII flux and the rest-frame UV luminosity predicted by Kennicutt (1998) :

$$\log[OII] = -0.4M_{UV} + 10.57 - \frac{DM(z)}{2.5} \quad (5)$$

It shows very good agreement between VVDS data from Lamareille et al. (2008) and the simulated emission lines strength extrapolated from the photometric redshift best fit template between $0.4 < z < 1.4$ where the OII emission line can be measured. Figure 9 shows the UV-OII relation using the VVDS data from Lamareille et al. (2008) with 4 color cuts corresponding to the early types in red circles, intermediate types in orange triangle, late types in square green and starburst galaxies in blue stars. Criteria for the type selections follows the Dahlen prescription detailed in the Table 1. This shows that the correlation has no strong dependence on the galaxy types. The histograms shown in Figure 10 are the emission line ratios

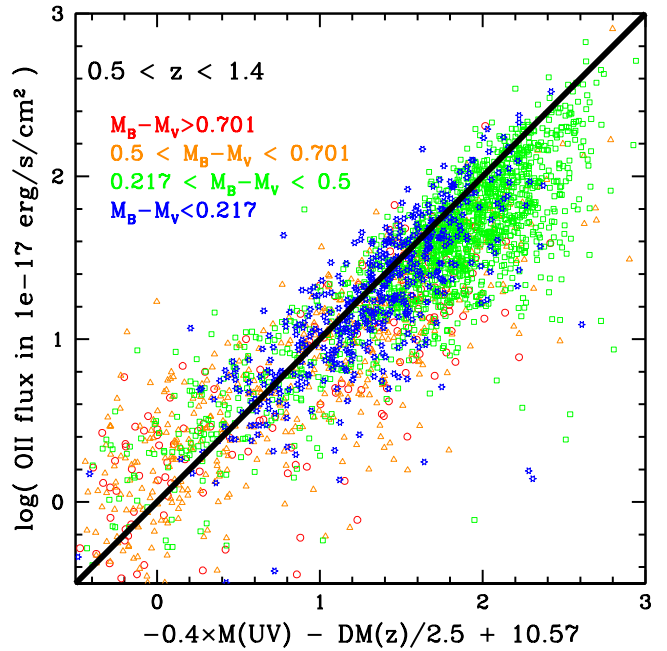


Fig. 9. UV-OII correlation using 4 color cuts representing the early, intermediate, late and starburst galaxies using the VVDS data from Lamareille et al. (2008).

of the CMC compared with those of VVDS. The attenuation causes a spread on the emission line ratios but we had to add a Gaussian dispersion to fit the VVDS emission line spread. If r_n is a set of n numbers randomly drawn from a Gaussian distribution $(\mu, \sigma^2) = (0, 1)$, we define the new fluxes as :

$$H\alpha = H\alpha(1 + |r_0/4|) \quad (6)$$

$$H\beta = H\beta(1 + |r_0/2|) \quad (7)$$

$$[OIII]_{4959} = [OIII]_{4959}(1 + |1.2r_1|) \quad (8)$$

$$[OIII]_{5007} = [OIII]_{5007}(1 + |r_2|) \quad (9)$$

We use the same random number r_0 to spread $H\alpha$ and $H\beta$ in order to preserve the ratio of these lines.

The spectral wavelength range of VVDS spans from 0.55 to $0.94\mu\text{m}$ (Le Fèvre et al. 2005) making the $[OII]$ line visible from redshift 0.5 to 1.5 and the $H\alpha$ line visible from redshift 0 to 0.5.

Thus we choose to evaluate the validity of the $H\alpha$ fluxes using the ratio $H\alpha/H\beta$, known as the Balmer decrement and having a value ~ 2.9 . The spread of the CMC emission line ratios fits well the emission line spread observed in the VVDS data.

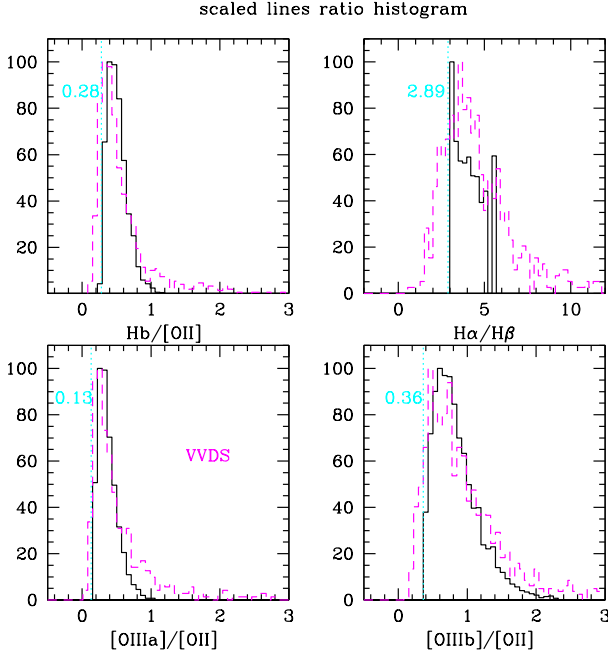


Fig. 10. Emission line ratios for the CMC catalog in black solid line compared to VVDS ratios in magenta dashed line. The cyan dotted line is the value of the theoretical emission line ratios.

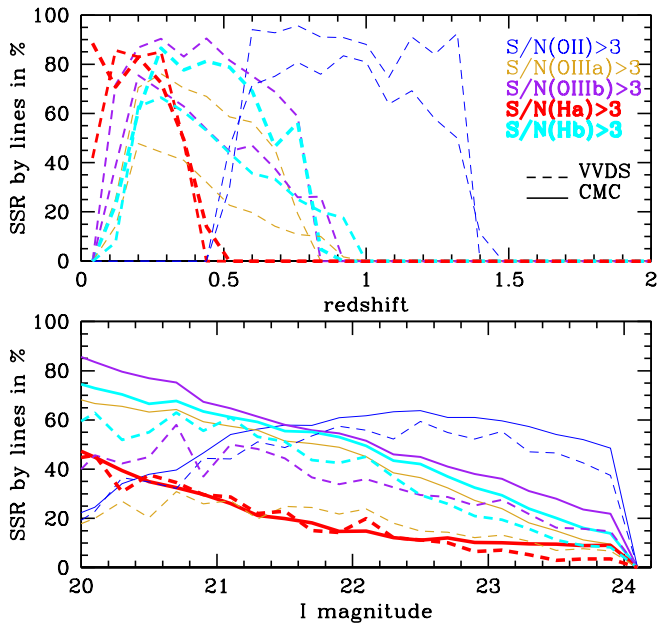


Fig. 11. Comparison of the lines Spectroscopic Success Rate (SSR) of the VVDS survey with the simulated lines VVDS SSR using the CMC emission lines.

For a further validation of the CMC emission lines we choose to reproduce the spectroscopic success rate (SSR) of the VVDS survey. To realise the CMC(VVDS) SSR we have extrapolated the flux sensitivity of the VVDS survey as a function of wavelength for several signal-to-noise ratio based on the [OII] emission lines. Using these sensitivities and the CMC emission line catalog we derive the simulated SSR for the VVDS survey in order to validate the emission line model of the CMC catalog (Figures 11 and 12). **Figures 11** show the SSR for the emission lines of the CMC catalog compared to those of the VVDS as a function of redshift and magnitude. The top panel shows the SSR of emission lines as a function of redshift, dashed lines for the VVDS survey and solid lines for the CMC. The blue lines are for the OII lines, red for $H\alpha$, cyan for $H\beta$, gold for OIIIa at 4959Å and purple for OIII at 5007Å using a growing thickness for each one in that order. The bottom panel shows the same as the top panel as a function of magnitude. The strong emission lines, $H\alpha$ and OII, are in very good agreement with the VVDS both in magnitude and redshift space. However weaker emission lines have a discrepancy of 10 to 20 % compared to the VVDS emission lines at low magnitudes, especially for the [OIII] lines at 4959Å and 5007Å, but it agrees very well at magnitudes $I > 21$. **Figures 12** compare the overall SSR predictions of the CMC with the VVDS secure and very secure redshifts. The top panel shows the VVDS SSR for secure redshift (brown thin lines) and very secure redshift (orange thick line) as a function of redshift compared to the CMC-VVDS emission lines 3σ flux detection (grey thin lines) and 2 lines at 5σ detection or OII at 5σ detection with $V < 24$ (magenta thick lines). The bottom panel shows the same as the bottom panel as a function of magnitude. We see that the VVDS secure redshifts success rate is very close to the 3σ detection line of the CMC catalog. In the same way, the VVDS very secure redshift success rate agrees very well with the 2 lines detection at 5σ . This includes galaxies with $V < 24$, which corresponds to a detection of the continuum in the VVDS spec-

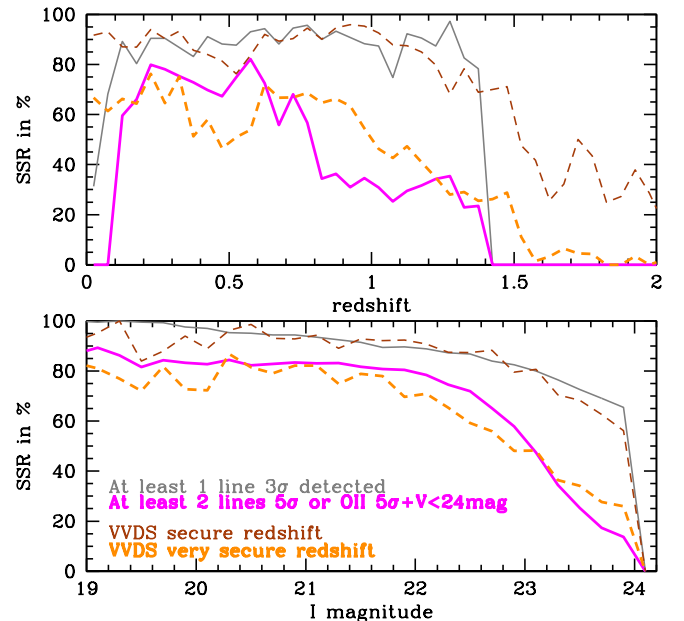


Fig. 12. Comparison of the Spectroscopic Success Rate (SSR) of the VVDS survey with the simulated VVDS SSR using the CMC emission lines.

tra with a $S/N > 10$ in the blue part of the spectrum (which is free of strong sky emission lines). The differences mainly comes from the redshifts effectively obtained using absorption lines for which the shape of the continuum altogether does not match exactly with our ad-hoc V-band magnitude criterion. Although the CMC does not simulate the absorption lines, we can say that the CMC emission line shows a good agreement both in redshift and magnitude with the VVDS spectroscopic survey. These results makes us confident in using the CMC catalog as a tool to predict the SSR of future wide field spectroscopic surveys.

4. Discussion

Different cosmological tests have been proposed to probe the geometry and growth of structures in order to shed new light on the nature of dark energy. The best approach is certainly to combine different probes to reduce the errors and better understand the systematics. However, each probe has its own requirements and it is a technical and scientific challenge to design a telescope optimised for more than one cosmological probe. Nonetheless, the goal of future dark energy programs should find a survey strategies that will lead to the best combined efficiency of different probes.

Having a realistic description of galaxy properties in our Universe is key to properly forecast what future deep and wide surveys can achieve for a given survey configuration. In this section, we start a discussion with requirements for a dark energy survey that combines shape measurements and a photo-z calibration survey (PZCS) for weak lensing with a BAO survey.

Thus, we will discuss two important aspects of these future dark energy mission: (i) the impact of galaxy size in terms of shape measurement for weak lensing depending on the PSF size (ii) the different typical WL and BAO survey configurations we have tested using our mock catalogues and (iii) their expected spectroscopic success rate.

Note that we are not conducting here any optimisation of such a space mission and its survey strategy. We are just putting in place some of tools necessary for such an optimisation.

4.1. Galaxy-sizes

A comparison of the simulated galaxy-size distribution to observational data is not particularly useful. Indeed the simulated catalogs agree, by construction, with the size distribution measured in the COSMOS ACS imaging survey (Koekemoer et al. 2007), (Leauthaud et al. 2007). No other survey capable of resolving faint galaxies approaches the size of the COSMOS/ACS data. In **Figure 13** we show the cumulated half-light radius distribution for the COSMOS data by bins of magnitude (different colors and thickness).

The brown area corresponds to the typical PSF size of ground-based telescopes. It shows that we can only resolve and measure galaxy shapes (those galaxies with a size larger than the PSF size) for about $15\text{gal}/\text{arcmin}^2$ (or up to $20\text{gal}/\text{arcmin}^2$ in case of excellent seeing) as soon as a depth of $I \sim 25$ is reached. Going deeper than $I = 25$ will not help to raise this number density as fainter galaxies are smaller than the PSF, thus making a shape measurement extremely difficult.

The grey area corresponds to the PSF size expected with future space Dark Energy mission; the exact value of the PSF size depends on the telescope diameter and the chosen pixel scale (here we assume a telescope diameter of $\sim 1.5 - 1.8$ meter). Interestingly, with this small PSF size, the number density of resolved galaxies does increase as a function of the depth of the

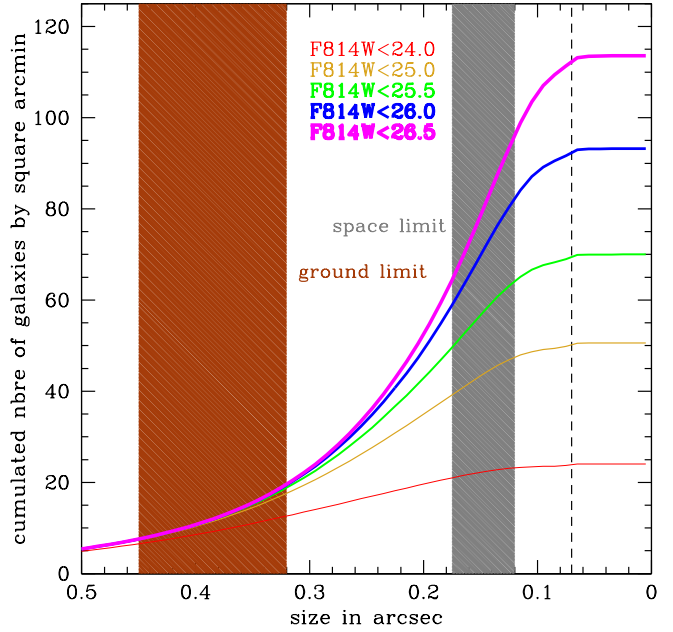


Fig. 13. Comparison of a ground-based and space weak-lensing survey using the COSMOS cumulated half-light radius distribution by bins of magnitude.

survey. Beyond $I = 26$ the increase in number density is however smaller, suggesting that there is a limited gain to go much deeper than $I = 26$ except perhaps for telescope designs with the smallest PSF size. With a depth of $I \sim 25.5 - 26$ the number density of resolved galaxies in the foreseen space surveys is about $3\times$ larger than what ground-survey can achieve.

Contrary to the ground case, the performance of a space survey in terms of galaxy number density critically depends both the depth and the resolution of the images. The black dashed vertical line correspond to the PSF size of the ACS/HST camera as measured in the COSMOS survey Leauthaud et al. (2007). The COSMOS survey reach a number density of resolved galaxies of $\sim 110\text{gal}/\text{arcmin}^2$ down to $I \sim 26.5$. It is important to recognize however that not all these galaxies could be used in the COSMOS 3D weak lensing analysis, as explained in Leauthaud et al (2007). For a fraction of these galaxies there was no counterpart in the ground-based catalogue because of masking of the data. For the remaining galaxies, it was not always possible to determine securely the shape or the redshift thus decreasing further the number of usable galaxies to roughly $40\text{gal}/\text{arcmin}^2$.

Cosmological weak lensing survey aim to maximize the number of resolved galaxies that can be used for weak lensing tomography. As shown by Amara & Réfrégier (2007), it is more efficient to conduct a wider survey than a deeper survey as the galaxy number increase is larger for a given exposure time by going wide than by going deep. However, the increase of Galactic absorption and stellar density, when getting closer to the Milky Way plane, will limit the gain of going wider than deeper when surveying areas larger than $\sim 15\,000\text{sq.deg}$.

4.2. BAO and WL spectroscopic survey requirements

We investigate here three types of spectroscopic redshift surveys, as can be seen in **Figure 14 and Table 4**), whose characteristics correspond to typical requirements for the BAO

and WL probes.

(i) BAO aims to measure the baryon acoustic oscillation peak of the 2-pt correlation function as a measure of a standard ruler. It requires a large survey area to reduce the statistical noise (Glazebrook & Blake 2005; Blake & Glazebrook 2003) and an accurate redshift for each galaxy, typically using spectroscopic techniques to reach a higher accuracy. One can use photometric redshifts instead of spectroscopic redshifts, but the loss of line-of-sight information then requires a few times larger area to reach the same dark energy figure of merit (FOM) Glazebrook & Blake (2005). Following this last paper, we investigate a WIDE near infrared (1.0 to 1.7 micron) spectroscopic survey reaching a 3σ sensitivity of $1 \times 10^{-16} \text{ ergs cm}^{-2} \text{ s}^{-1}$ at $1.2 \mu\text{m}$ (this can be achieved with an efficient slitless spectrograph using a 1.5m telescope, $0.28''/\text{pixel}$, $R \sim 500$ and an exposure time of 1200 sec) and covering a large area on the sky to maximise the dark energy FOM. The flux sensitivities of such a survey are represented by the solid cyan (and high thickness) line in **Figure 14**.

(ii) The weak-lensing tomographic analysis is likely the most efficient lensing method to estimate the dark energy parameters (Massey et al. 2007; Amara & Réfrégier 2007). This method probes the growth of structures but needs to have accurate redshifts to place the background sources at their correct location. To achieve this measurement, it is essential to determine with the best accuracy (and minimal biases) the photometric redshift (photo-z) of all the galaxies to be used in the weak lensing tomography. Ma & Bernstein (2008) have shown that a high accuracy photo-z is needed to avoid any bias on the Dark Energy parameter estimation. The only way to reach high accuracy photo-z is to plan a spectroscopic redshift survey to calibrate the photo-z templates, as in Ilbert et al. (2006). Ideally, the photo-z calibration survey (PZCS) would reach the same magnitude and redshift depth as the WL photometric survey. However, this goal will likely be difficult to achieve and the CMC emission-line catalog may help to plan the best spectroscopic strategy. Thus, we design a DEEP-visible-NIR survey (0.6 to 1.7 microns) for weak-lensing, reaching a 3σ flux sensitivity of $5.10^{-18} \text{ ergs cm}^{-2} \text{ s}^{-1}$ at $1.2 \mu\text{m}$ (this can be achieved with an efficient slitless spectrograph using a 1.5m telescope, $0.28''/\text{pixel}$, $R \sim 250$ and an exposure time of 240 ksec ~ 67 hours) as an attempt at calibrating photometric redshifts for a wide range in redshift and magnitude. The flux sensitivities of such a survey are represented by the solid red (and medium thickness) line for a 5σ detection and by the solid black (and thin) line for a 3σ detection in **Figure 14**.

(iii) We also design a DEEP-NIR survey having the same characteristics as the DEEP-visible-NIR survey but covering only the NIR part (1.0 to 1.7 micron; focussing on the low IR background of space observation). Our goal here is to evaluate the importance of having a spectroscopic contribution in the visible wavelength to reach a high completeness.

In **Figure 14**, we also represent the VVDS-DEEP flux sensitivities in green (and thin) dashed line for a 3σ detection and gold (and thick) dashed line for a 5σ detection. For reference, the exposure time of the VVDS-DEEP survey is ~ 10 ksec exposure on a 8m ground-based telescope with a spectroscopic resolution of $R=250$.

4.3. SSR prediction

In the following sections we will give the basics of photo-z calibrations survey studies based on the spectroscopic success rate

as a function of redshift and magnitude. A more thorough analysis will be developed in a forthcoming paper (Jouvel et al 2009 in prep).

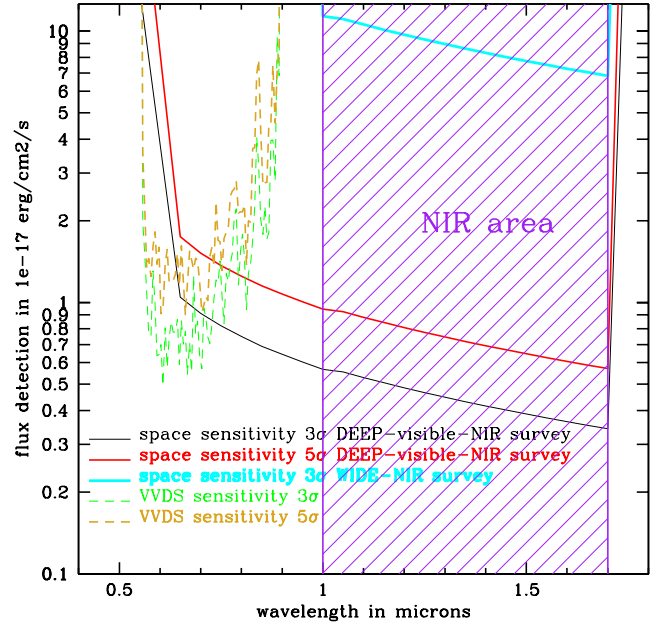


Fig. 14. Flux sensitivities for the VVDS-DEEP survey as a function of wavelength compared to forecast of future space WIDE and DEEP NIR [purple and shaded area] surveys with or without visible coverage.

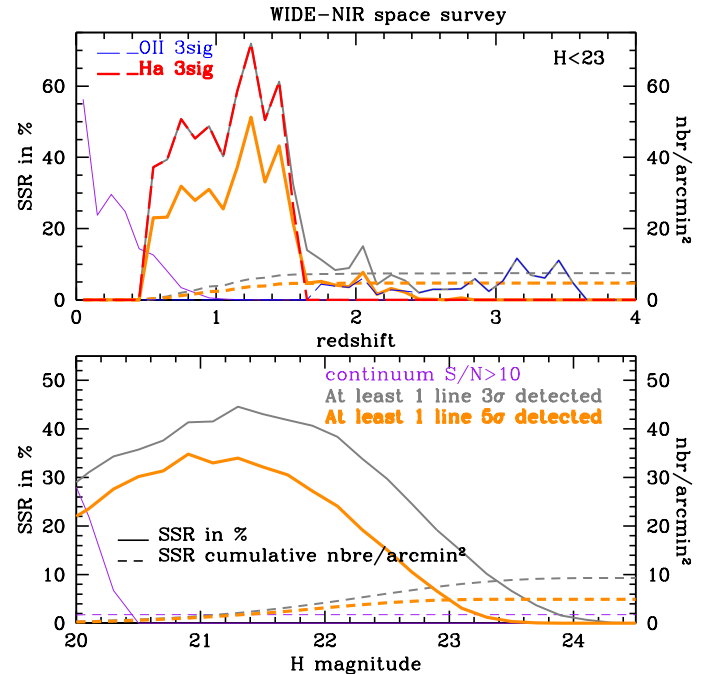


Fig. 15. WIDE NIR space survey SSR.

4.3.1. SSR for the WIDE survey

Figure 15 shows SSR forecasts for a future NIR WIDE survey. Top panel represents the SSR as a function of redshift and bottom panel as a function of magnitude. Both panels show the SSR using a one line at 5σ detection criterion in orange very thick, a one line at 3σ detection criterion in grey thick, and a continuum $S/N > 10$ criterion in purple thin. The solid curves are a percentage with the total number of objects and the dashed for a cumulative number of objects by arcmin². The top panel shows also the SSR of a 3σ detection of the OII emission line in blue long-dashed thin line and $H\alpha$ in red long-dashed thick line. The wide survey would aim to cover a large fraction of the sky (10,000 deg² or more) in order to probe the large scale distribution of galaxies aiming in particular to measure the baryon acoustic oscillation with a great accuracy in the redshift range $0.5 < z \leq 1.5$ (or up to $z \sim 2$ providing the telescope and instrument is sensitive up to $2\mu\text{m}$). Our SSR prediction, shows that such survey could easily measure the redshift of more than 4 galaxy/arcmin² hence providing the redshift measurement of more than ~ 100 million galaxies for a survey covering 10,000 deg². The redshift identification is essentially based on the $H\alpha$ line detection thus essentially targeting star-forming galaxies with $H \lesssim 22.5$. The SSR clearly shows that such survey is far from being complete as the spectroscopic success rate is generally below 40% for any magnitude and redshift (for a 5σ line detection). Indeed, there are very few faint galaxies with spectroscopic success, especially in the redshift ranges which have the strongest need for photometric redshift calibration : $0 < z < 0.5$ and $z > 1.5$. Table 4 shows that the SSR also depends strongly on galaxy type. Thus, the wide survey *can not be used* to calibrate any photometric redshift catalogue properly.

4.3.2. SSR for the DEEP survey

Figure 16 and 17 show the SSR prediction for future dark energy surveys which are planning to do infrared only (DEEP-NIR survey), and visible+infrared spectroscopy (DEEP-visible-NIR survey) from space. Figure 14 shows the grism flux sensitivities we use in our analysis. It shows SSR as a function of redshift [top panel] and magnitude [bottom panel]. Both panels show the SSR using a 2 lines detection with at least one line at 5σ detection criterion in orange very thick, a one line at 3σ detection criterion in grey thick, and a continuum $S/N > 10$ criterion in purple thin. The solid curves are a percentage with the total number of objects and the dashed for a cumulative number of objects by arcmin². The top panel shows also the SSR of a 3σ detection of the OII emission line in blue long-dashed thin line and $H\alpha$ in red long-dashed thick line.

We assume here that the visible spectroscopy spans $0.6\text{--}1\mu\text{m}$ see Figure 14. Because of the limited wavelength coverage, the $H\alpha$ is the only strong emission line visible for galaxies at low redshift ($z < 0.5$). This explains that the detection criterion based on 2 lines, does not cover the low redshift range as shown in the top panel of Figure 16. This is also seen in the bottom panel of Figure 16 where there is a lower SSR for bright galaxies. However, for these low redshift ($z < 0.5$) galaxies, about 30% have a strong continuum with $S/N > 10$. For these bright galaxies, we should be able to accurately measure a redshift using either the $H\alpha$ line detection, absorption lines and the shape of the continuum which will be useful for photometric redshift calibration.

If only the NIR spectroscopy is conducted from space, the survey will only reach ~ 35 galaxy per arcmin² and a maximal SSR of at best 40% for $I \sim 24$. Using DEEP-NIR spectroscopic

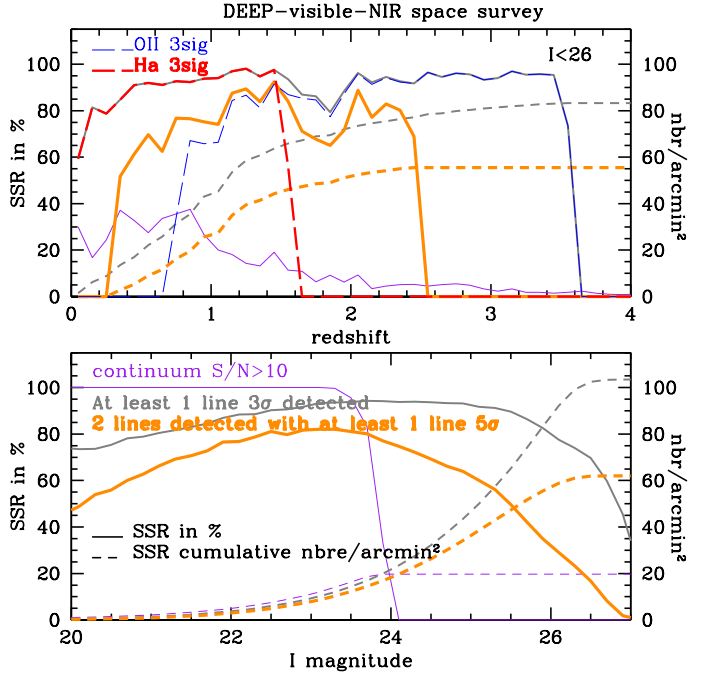


Fig. 16. DEEP-visible-NIR space survey SSR.

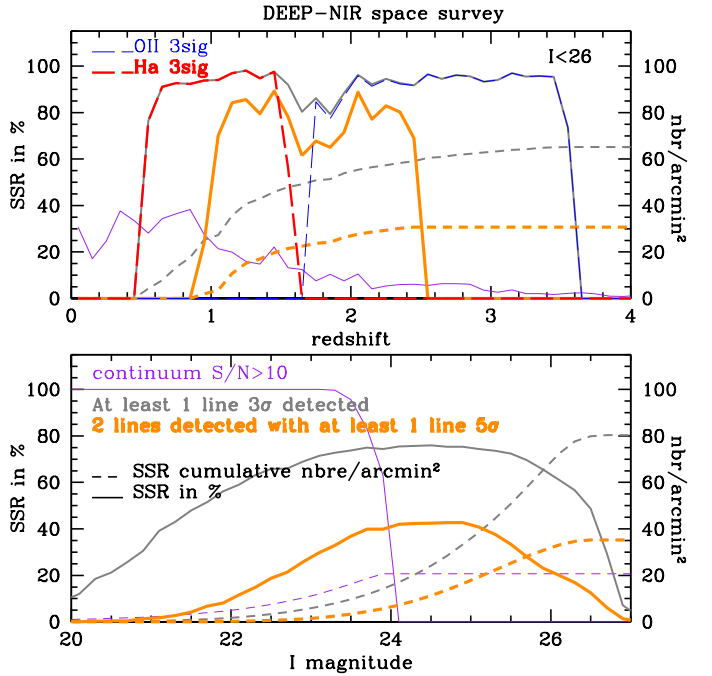


Fig. 17. DEEP-NIR only space survey SSR.

survey would help to calibrate spectra at $0.8 < z < 2.5$ but would be less efficient below $z < 0.8$. There will be a strong need to conduct visible spectroscopy to achieve a complete census of the redshift distribution.

Using the DEEP-visible-NIR survey, we should be able to measure a very secure redshift (2 lines detected at more than 3σ with at least 1 emission line at 5σ) for about 60 galaxy per arcmin² to $I < 26$ and $z \lesssim 2.5$ with a SSR reaching 80% at best for $I \sim 24$. With this density of sources, a survey of 1 square degree will provide 220000 spectra. Note, however, that these numbers do not take into account the crowding of galaxy spec-

tra which is likely a strong limiting factor above $I \sim 24$. There are ways to minimize the impact of crowding, for example by conducting the slit-less spectroscopic survey using different orientations, or by using masks to block some of the light (thus limiting the sky background and reducing the number of overlapping spectra). These alternatives will be discussed in a forthcoming paper (Zoubian et al. 2009 in prep.). Note also that the visible part of the spectroscopy might be conducted with a dedicated ground-based spectrograph with high multiplexing. This can probably be especially more efficient for $\lambda < 0.75\mu\text{m}$ where the sky emission lines are less numerous than in the redder part of the spectrum.

Table 4. Characteristics of the three surveys discussed in the text, assuming an efficient 1.5m space telescope with an obscuration of 0.6m and a total telescope throughput (CCD, mirror, grism) of 70% using a survey efficiency of 75%. The % [1line3 σ] Ell represent the percentage of Elliptical galaxies spectroscopically found using a success criterion of 1 line detected at 3 σ compared to the total population of Elliptical galaxies. With the same criterion, we define the percentage of Sac for early spiral galaxies, Sdm for late spiral galaxies, and SB for starburst galaxies.

	DEEP-vis-NIR	DEEP-NIR	WIDE-NIR
probe	WL	WL	BAO
T_{obs}	240ksec	240ksec	1200sec
λ in μm	0.6-1.7	1-1.7	1-1.7
3σ at $1.2\mu\text{m}$	5.10^{-18}	5.10^{-18}	1.10^{-16}
		$\text{ergs cm}^{-2} \text{sec}^{-1}$	
area needed	10deg^2	10deg^2	20000deg^2
mission time	0.2yrs	0.2yrs	2yrs
		FOV of 0.5deg^2	
nbr density (5σ)	60	35	5
		gal/arcmin^2	
z [1line3 σ]	$0 < z < 3.5$	$0.5 < z < 3.5$	$0.5 < z < 1.5$
m_{lim} [1line3 σ]	$I \sim 27$	$I \sim 26.5$	$H \sim 22$
% [1line3 σ] Ell	40	27	0
% [1line3 σ] Sac	60	51	1
% [1line3 σ] Sdm	77	63	10
% [1line3 σ] SB	95	74	45

5. Conclusion

We have produced simulated deep galaxy catalogs by two different techniques: one starts with redshift-dependent Schechter luminosity functions for three galaxy types for $0 < z < 6$, extrapolating the LFs derived from GOODS data by Dahlen et al. (2005) (the GLFC). The other has galaxies with redshifts and SEDs taken as the best photo-z fits to multiwavelength observations of the COSMOS field (the CMC). Both adopt galaxy size distributions from the COSMOS HST imaging and we assign emission line strengths using a recipe in agreement with the VVDS-DEEP data.

Both simulated catalogs do an excellent job of reproducing the dN/dm data ($< 20\%$ discrepancies) and color distributions (0.1–0.2 mag median color discrepancies) of galaxies observed in bands from 0.4 to $2.2\mu\text{m}$ using a comparison with the GOODS and UDF surveys. The CMC provides an excellent match to the redshift-magnitude and redshift-color distributions for $I < 24$ galaxies in the VVDS spectroscopic redshift survey.

These simulated catalogs thus pass all our validation tests for use in forecasting the galaxy “yields” of future visible/NIR imaging surveys, as long as we restrict our analysis to the $I < 25.5$ – 26 galaxies for which the COSMOS HST imaging is highly complete. These simulated catalogs provide a conservative estimate of the yield for surveys that go deeper in the visible, or reach > 24 in the NIR, because they miss the faint or red galaxies that do not make the I -band cut.

The GLFC has the potential to forecast deeper surveys than the CMC, but only if we are ready to extrapolate the luminosity functions to fainter magnitudes, which is probably feasible in the visible bands, but may be more strongly limited in the near-infrared bands.

In the CMC, the galaxy sizes are directly coming from the HST/ACS measurement and give us the opportunity to evaluate differences in terms of possible shape measurements for a ground-based and space telescopes. A ground based WL survey is limited to use only the resolved galaxies, and we show that most $I > 25$ galaxies are smaller than the ground-based seeing disk. Thus the WL depth of ground-based surveys is basically independent of the survey depth for $I > 25$. For a space survey the number of resolved galaxies is not only dependent on the PSF but also on the depth of the survey.

Moreover we have also used the CMC and the emission line model to compare the spectroscopic success rate observed by the VVDS and the one we can predict based on the CMC line fluxes. In general we obtain a good agreement between observed success rates and the CMC predictions.

We have then used the emission line model to explore what will be the yield in terms of redshift measurements for 2 type of surveys: (i) a WIDE survey motivated by measuring BAO, and (ii) a deep survey motivated to calibrate photometric redshifts. We found that the WIDE survey reaches a density of 4gal/arcmin^2 for galaxies $H \lesssim 22.5$ in a redshift range of $0.5 < z < 1.5$ mainly detected using the $H\alpha$ emission line. Furthermore, in a weak-lensing perspective, a DEEP survey both visible and NIR is needed to conduct a photometric redshift calibration of galaxies (PZCS) to be used in a weak-lensing measurement covering the full magnitude and redshift range. Indeed such survey reaches a density of 60gal/arcmin^2 for very secure redshifts down to $I \sim 25.5$ with a high completeness of $\sim 80\%$. We note that the visible part of the spectroscopic survey can be done from the ground, however above $\lambda \sim 0.75\mu\text{m}$ a space survey is likely to be much more efficient than a ground-based survey (see Figure 14).

We have thus demonstrated here how useful realistic simulated catalogs are for designing future DE space missions. We will investigate more precisely details of the WL optimisation survey strategy in a forthcoming paper (Jouvel et al. 2009, in prep.).

Acknowledgements. We acknowledge useful discussions with members of the COSMOS and SNAP collaborations. Stephanie Jouvel thanks CNES and CNRS for her PhD studentship. Jean-Paul Kneib thanks CNRS for support. Gary Bernstein is supported by grant AST-0607667 from the National Science Foundation, Department of Energy grant DOE-DE-FG02-95ER40893, and NASA grant BEFS-04-0014-0018.

References

- Amara, A. & Réfrégier, A. 2007, MNRAS, 381, 1018
- Astier, P., Guy, J., Regnault, N., et al. 2006, A&A, 447, 31
- Blake, C. & Glazebrook, K. 2003, ApJ, 594, 665
- Calzetti, D., Armus, L., Bohlin, R. C., et al. 2000, ApJ, 533, 682
- Capak, P., Aussel, H., Ajiki, M., et al. 2007, ApJS, 172, 99
- Coe, D., Benítez, N., Sánchez, S. F., et al. 2006, AJ, 132, 926

- Coleman, G. D., Wu, C.-C., & Weedman, D. W. 1980, *ApJS*, 43, 393
- Dahlen, T., Mobasher, B., Jouvel, S., et al. 2008, *AJ*, 136, 1361
- Dahlen, T., Mobasher, B., Somerville, R. S., et al. 2005, *ApJ*, 631, 126
- Giavalisco, M., Ferguson, H. C., Koekemoer, A. M., et al. 2004, *ApJ*, 600, L93
- Glazebrook, K. & Blake, C. 2005, *ApJ*, 631, 1
- Grazian, A., Fontana, A., de Santis, C., et al. 2006, *A&A*, 449, 951
- Ilbert, O., Arnouts, S., McCracken, H. J., et al. 2006, *A&A*, 457, 841
- Ilbert, O., Capak, P., Salvato, M., et al. 2009, *ApJ*, 690, 1236
- Iovino, A., McCracken, H. J., Garilli, B., et al. 2005, *A&A*, 442, 423
- Jouvel, S., Kneib, J.-P., Bernstein, G., et al. 2009, in prep.
- Kennicutt, Jr., R. C. 1998, *ARA&A*, 36, 189
- Kilbinger, M., Benabed, K., Guy, J., et al. 2009, *A&A*, 497, 677
- Koekemoer, A. M., Aussel, H., Calzetti, D., et al. 2007, *ApJS*, 172, 196
- Lamareille, F., Brinchmann, J., Contini, T., et al. 2008, *ArXiv e-prints*
- Lawrence, A., Warren, S. J., Almaini, O., et al. 2007, *MNRAS*, 379, 1599
- Le Fèvre, O., Vettolani, G., Garilli, B., et al. 2005, *A&A*, 439, 845
- Leauthaud, A., Massey, R., Kneib, J.-P., et al. 2007, *ApJS*, 172, 219
- Ma, Z. & Bernstein, G. 2008, *ApJ*, 682, 39
- Madau, P. 1995, *ApJ*, 441, 18
- Massey, R., Rowe, B., Refregier, A., Bacon, D. J., & Bergé, J. 2007, *MNRAS*, 380, 229
- McCall, M. L., Rybski, P. M., & Shields, G. A. 1985, *ApJS*, 57, 1
- McCracken, H. J., Radovich, M., Bertin, E., et al. 2003, *A&A*, 410, 17
- Mouhcine, M., Lewis, I., Jones, B., et al. 2005, *MNRAS*, 362, 1143
- Moustakas, J., Kennicutt, Jr., R. C., & Tremonti, C. A. 2006, *ApJ*, 642, 775
- Perlmutter, S., Aldering, G., Goldhaber, G., et al. 1999, *ApJ*, 517, 565
- Riess, A. G., Filippenko, A. V., Challis, P., et al. 1998, *AJ*, 116, 1009
- Sawicki, M. J., Yee, H. K. C., & Lin, H. 1996, *JRASC*, 90, 337
- Zoubian, J. & Kneib, J.-P. 2009, in prep.

Designing Future Dark Energy Space Mission: I. Building Realistic Galaxy Spectro-Photometric Catalogs and their first applications

S. Jouvel¹, J-P. Kneib¹, O. Ilbert^{3,1}, G. Bernstein², S. Arnouts^{1,4}, T. Dahlen⁵, A. Ealet^{9,1}, B. Milliard¹, H. Aussel⁷, P. Capak⁶, A. Koekemoer⁵, V. Le Brun¹, H. McCracken⁸, M. Salvato⁶, and N. Scoville⁶

¹ Laboratoire d'Astrophysique de Marseille, CNRS-Université d'Aix-Marseille, 38 rue Frederic Joliot-Curie; 13388 Marseille cedex 13, France

² University of Pennsylvania, 4N1 David Rittenhouse Lab 209 S 33rd St Philadelphia, PA 19104, USA

³ Institute of Astronomy, 2680 Woodlawn Drive Honolulu, HI 96822-1897, USA

⁴ CFHT, 65-1238 Mamalahoa Hwy Kamuela, Hawaii 96743 USA

⁵ Space Telescope Science Institute, 3700 San Martin Drive Baltimore, MD 21218 USA

⁶ California Institute of Technology 1200 East California Blvd. Pasadena CA 91125, USA

⁷ Service d'Astrophysique, CEA-Saclay, 91191 Gif-sur-Yvette, France

⁸ Institut d'Astrophysique de Paris 98bis, bd Arago F75014 Paris, France

⁹ Centre de Physique des Particules de Marseille, 163, avenue de Luminy, Case 902, 13288 Marseille cedex 09, France

DRAFT VERSION: MAY 29, 2009

ABSTRACT

Context. Future dark energy space missions such as JDEM and EUCLID are being designed to survey the galaxy population to trace the geometry of the universe and the growth of structure, which both depend on the cosmological model. To reach the goal of high precision cosmology they need to evaluate the capabilities of different instrument designs based on realistic mock catalog of the galaxy distribution.

Aims. The aim of this paper is to construct realistic and flexible mock catalogs based on our knowledge of galaxy population from current deep surveys. We explore two categories of mock catalog : (i) based on luminosity functions fit of observations (GOODS, UDF, COSMOS, VVDS) (ii) based on the observed COSMOS galaxy distribution.

Methods. The COSMOS mock catalog benefits from all the properties of the data-rich COSMOS survey and the high accuracy photometric redshift distribution based on 30 bands photometry. Nevertheless this catalog is limited to the depth of the COSMOS survey. Thus, we also evaluate a mock galaxy catalog generated from luminosity functions using the *Le Phare* software. For these two catalogs, we have produced simulated number counts in several bands, color diagrams and redshift distribution for validation against real observational data.

Results. Using these mock catalogs we derive some basic requirements to help designing future Dark Energy mission in terms of number of galaxies available for the weak-lensing analysis as a function of the PSF size and depth of the survey. We also compute the spectroscopic success rate for future spectroscopic redshift surveys (i) aiming at measuring BAO in the case of the wide field spectroscopic redshift survey, and (ii) for the photometric redshift calibration survey which is required to achieve weak lensing tomography with great accuracy. In particular, we demonstrate that for the photometric redshift calibration, using only NIR (1-1.7 μ m) spectroscopy we can not achieve a complete spectroscopic survey down to the limit of the photometric survey ($I < 25.5$). Extending the wavelength coverage of the spectroscopic survey to cover 0.6-1.7 μ m will then improve the fraction of very secure spectroscopic redshift to nearly 80% of the galaxies making then possible a very accurate photometric redshift calibration.

Conclusions. We have produced two realistic mock galaxy catalogs that can be used in studying the best survey strategy of future dark-energy missions in terms of photometric redshift accuracy and spectroscopic redshift surveys yield. *These catalogues are publicly accessible at <http://lamwww.oamp.fr/cosmowiki/RealisticSpectroPhotCat>, or by request to the first author of this paper.*

Key words. redshift – JDEM – cosmology – surveys – mock catalog

1. Introduction

The prospect for high-precision cosmological inferences from large galaxy surveys has prompted the initiation of several projects with the goal of surveying thousands of square degrees of sky in multiple filters and/or spectroscopy. The ground based projects [e.g. current KIDS, DES, and future Pan-STARRS, LSST in imaging and current SDSS-III/BOSS and future WFMOS BigBOSS in spectroscopy], and the space based missions [JDEM, and EUCLID, or their former and future con-

cepts] all propose to conduct wide field galaxy survey (in imaging and/or spectroscopy) in order to exploit the power of weak gravitational lensing [WL] and galaxy distribution (using baryonic acoustic oscillation [BAO] and/or the redshift distortion measurement [RD]) to elucidate the cause of the acceleration of the Hubble expansion (Riess et al. (1998), Perlmutter et al. (1999), Astier et al. (2006), Kilbinger et al. (2009)). Proper design and forecasting of the performance of these experiments requires an accurate estimate of the “yield” of galaxies, such as number counts, redshift size and color distribution, from a chosen survey configuration. It is typically straightforward to estimate the expected resolution and noise properties of the telescope and instrument, but more difficult to quantify the number

Send offprint requests to: Stephanie Jouvel, e-mail: stephanie.jouvel@oamp.fr

and properties of the “useful” galaxies available on the sky. A good forecast requires that we estimate the density of galaxies on the sky over the joint distribution of:

- (i) redshift; (ii) angular size, expressed as half-light radius $r_{1/2}$;
- (iii) apparent magnitudes and colors in any chosen instrument passbands; (iv) emission-line strengths.

The first three properties are essential to knowing whether a given galaxy will be detected at sufficient signal-to-noise (S/N) and resolution to determine its shape and its photometric redshift. The last property, the emission-line strength, is essential to estimating the depth and completeness that any spectroscopic redshift survey will achieve. Spectroscopic redshift accuracy is needed to conduct the best possible BAO/RD measurements, and to calibrate photometric redshift (“photo- z ”) estimators that are essential for WL tomographic measurement (e.g. Massey et al. (2007)).

In this paper we present two simulated catalogs of galaxy properties based on current deep surveys, that we will use in forthcoming papers (Jouvel et al. 2009 in prep.) to forecast the performance of WL Dark Energy space based mission. Unfortunately we cannot simply use a catalog from some completed survey, since (1) no single survey of useful depth has simultaneously observed all of the listed properties for its target galaxies, and (2) the proposed surveys will exceed the depth, field of view, resolution, and/or wavelength coverage of most existing observed galaxy catalogs. For example the space based spectroscopic survey will likely mainly be conducted in the near-infrared, surpassing any current infrared spectroscopic redshift survey. **The mission concepts of SNAP, Destiny, and EUCLID propose near-infrared (NIR) imaging over very wide areas but only a few square arcminutes of HST/NICMOS imaging data with the UDF (Coe et al. 2006) and close to one degree down to $K \sim 23$ for ground based data with the UKIDSS survey on the UKIRT telescope (Lawrence et al. 2007) are available to date at these magnitude levels, insufficient to serve as a robust source model.** Any relevant simulated catalogs must therefore include some degree of extrapolation or modelling of the source population.

In this paper, we explain how we have constructed, based on deep survey data, simulated galaxy catalog. Section 2 explain the methodology used. In section 3 we validate these simulated catalogs by comparing their predicted magnitude, color, redshift, size, and emission-line strength distributions to real survey data taking into account the survey selection functions.

Although this work was initiated in the context of the SNAP collaboration (see our first results in Dahlen et al. (2008)), it can easily be adapted to any instrument concept for a proper evaluation of its merit. When necessary we assume a Λ CDM universe: $(\Omega_M, \Omega_\Lambda) = (0.3, 0.7)$ and $H_0 = 70$ km/s/Mpc. All magnitudes used in this paper are on the AB system.

2. Realistic mock Galaxy Catalog

For both of our simulated catalogs, each galaxy is assigned a spectral energy distribution (SED), which can be integrated over any instrumental passband to forecast an apparent magnitude. Our first fully simulated catalog has been generated by using “Le Phare” simulation tool¹ (Arnouts and Ilbert 2009 in prep) with an analytic luminosity function based on the GOODS survey from the work of Dahlen et al. (2005). We will refer to our derived simulated catalog as the *GOODS Luminosity Function Catalog (GLFC)*.

¹ Arnouts http://www.oamp.fr/people/arnouts/LE_PHARE.html

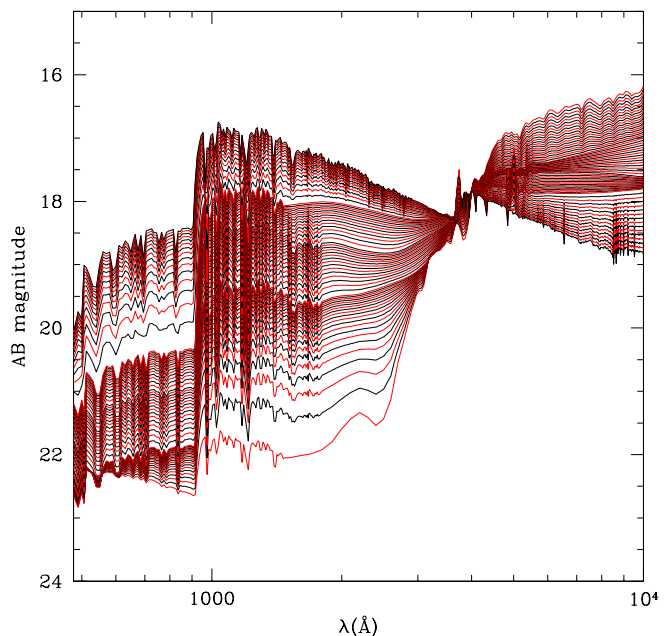


Fig. 1. Extended CWW library of SED templates. This represents the full range of SED template linearly interpolated between the 4 CWW templates and one star-forming template in AB magnitude (arbitrarily flux scaled at 4000\AA).

2.1. GLFC - GOODS Luminosity Function based Catalog

2.1.1. SED Library

The GLFC relies on two ingredients :

- A sub-class of SED spanning the entire range from Elliptical to starbursting galaxy,
- A redshift evolving luminosity function (LF) per type.

Those ingredients are the basic requirements to generate a catalog that can predict global distributions such as magnitude, redshift and colors counts. We use the Coleman Extended library (CE) for our templates of galaxies. This list is based on the four observed spectra of Coleman et al. (1980) corresponding to an Elliptical, Sbc, Scd and Irregular, which have been extrapolated in the UV and IR wavelengths domain by using synthetic spectra from the GISSEL library (Charlot and Bruzual, 1996). To reproduce observed colors bluer than the CE templates, we add one spectrum of star-forming galaxies computed with the GISSEL model for solar metallicity, Salpeter IMF, constant star formation rate and 0.05 Gyr age. Following the approach adopted by Sawicki et al. (1996), we have linearly interpolated the original 5 SEDs to provide a finer grid of spectral-type coverage with a total library of 66 templates shown in Figure 1.

2.1.2. Extinction

We have diversified our templates in adding extinction coming from the Calzetti extinction law (Calzetti et al. 2000) with the excess reddening values $E(B - V)$ of 0, 0.1, 0.2, 0.3 mag using the extinction formula:

$$flux_{attenuated}(\lambda) = flux_{intrinsic}(\lambda) \cdot 10^{-0.4 * k(\lambda) * E(B-V)} \quad (1)$$

The $k(\lambda)$ values follow the Calzetti law. Each $E(B - V)$ value will be used to create a template adding diversity to the templates already existing. This has been applied to the irregular

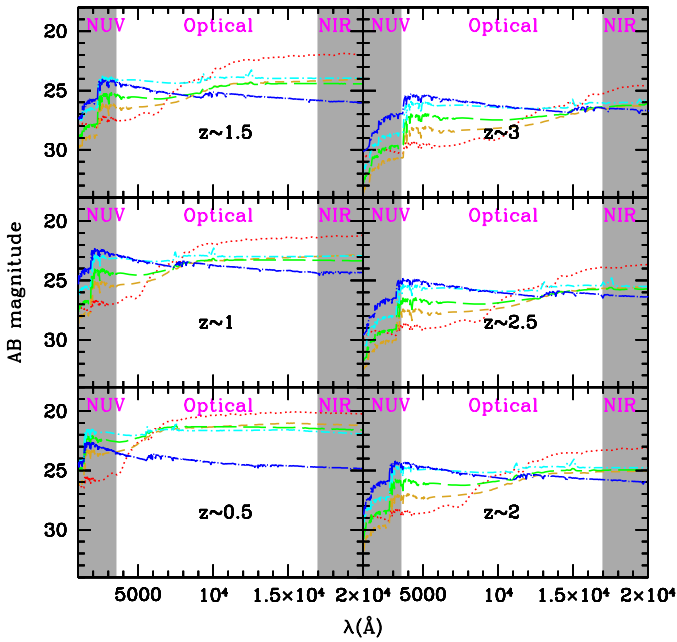


Fig. 2. Four of the CWW templates: Ell (red dotted), S_{bc} (gold dashed), S_{cd} (green long-dashed), Irr (cyan dot-dashed) and the star-forming (blue long dot-dashed) shown at some given redshift of 0.5, 1, 1.5, 2, 2.5, 3. The templates are M^* galaxies as given in Table 2. This is useful to show the color of these templates which may help in deciding which sensitivities are needed to detect galaxies in different passbands.

Table 1. Restframe colors of SED templates.

LF	E(B-V)	types	$B - V(\text{restframe})$
1	0	1 \rightarrow 17	1.069 \rightarrow 0.701
2	0	17 \rightarrow 55	0.701 \rightarrow 0.2167
3	0	55 \rightarrow 66	0.2167 \rightarrow -0.0301
3	0.1	56 \rightarrow 66	0.3252 \rightarrow 0.1016
3	0.2	56 \rightarrow 66	0.4592 \rightarrow 0.2345
3	0.3	56 \rightarrow 66	0.5945 \rightarrow 0.3686
Main templates	E(B-V)	nbr	$B - V(\text{restframe})$
Ell	0	1	1.069
S_{bc}	0	21	0.6262
S_{cd}	0	36	0.5077
Irr	0	51	0.3185
$star - forming$	0	66	-0.0301

and star-forming templates increasing the number of templates for those types. Finally we also include the Lyman absorption by Intergalactic Medium as a function of redshift following Madau (1995).

2.1.3. GLFC Luminosity Function

The GLFC is generated by assuming a luminosity function (LF) for galaxies of 3 different types, then drawing galaxies from these LFs to populate our simulated sky area. We have selected these 3 types following the B-V restframe colors given in Dahlen et al. (2005) (see table 1). We start with the LF estimated in restframe B band by Dahlen et al. (2005) in the 3 spectral types inside 4 redshifts bins over $0 < z < 1$. Dahlen et al. (2005) derive these LFs by fitting to photo-z data from the GOODS survey.

We have extrapolated these LFs to $z = 6$ to be complete for the galaxies likely to be used in future surveys. The Dahlen $z = 1$ LF for each type is held nearly fixed for $1 < z < 6$, with some adjustments made to improve the match to data from the COSMOS survey (described below).

Table 2 gives the LF calculated for 3 galaxy types extrapolated until redshift $z \approx 6$ as explained above. To produce the mock catalog, knowing the luminosity function, Le Phare derives a number of object by magnitude and redshift bin (z, m) using a Schechter function (Schechter 1976) :

$$n(M(z, m))dM = \phi^* \left(\frac{M(z, m)}{M^*} \right)^\alpha \exp \left(-\frac{M(z, m)}{M^*} \right) \frac{dM}{M^*} \quad (2)$$

M is the absolute magnitude which is a function of redshift and apparent magnitude (z, m), M^* , ϕ^* and α are the parameters of the Schechter function given in the table 2.

According to the adopted area, the simulated galaxy counts in each magnitude-redshift-type bin are drawn from a Poisson distribution of the expected number based on the LF.

Note that the luminosity function parameters depend on the cosmological model assumed (as the luminosity function is expressed in physical units), however the resulting galaxy catalog can be considered independent of the input cosmological parameters assumed here, as it is built to reproduce the *observed* galaxy distribution and properties.

Table 2. Luminosity function in the B band extrapolated to match COSMOS colors and number counts. Those values are the one used in GLFC.

LF	z	ϕ^*	M^*	α
1	0.5	16.7e-4	-21.15	-0.71
1	0.75	18e-4	-21.13	-0.50
1	1.0	9.5e-4	-21.72	-0.98
1	2.0	8.5e-4	-21.72	-0.98
1	3.0	7.5e-4	-21.72	-0.98
1	6.0	6.5e-4	-21.72	-0.98
2	0.5	24.0e-4	-21.08	-1.37
2	0.75	25.0e-4	-21.29	-1.17
2	1.0	25.0e-4	-21.2	-1.1
2	1.5	24.4e-4	-21.15	-0.05
2	2.0	24.4e-4	-21.15	-0.99
2	3.0	24.4e-4	-21.15	-0.99
2	6.0	24.4e-4	-21.15	-0.85
3	0.5	48.6e-4	-18.84	-1.1
3	0.75	33.1e-4	-19.67	-1.18
3	1.0	33.1e-4	-20.55	-1.52
3	1.5	30.0e-4	-20.62	-1.62
3	2.0	25.0e-4	-20.72	-1.7
3	3.0	25.0e-4	-20.72	-1.8
3	6.0	25.0e-4	-20.72	-1.8

Drawing from the luminosity functions gives the galaxy distribution over the joint magnitude-color-redshift space. We assign a half-light radius to each galaxy as follows: we first calculate the galaxy's apparent magnitude in the F814W HST filter. Leauthaud et al. (2007) provides a size-magnitude catalog for the 1.64 deg² COSMOS survey executed in this filter. We assign the simulated galaxy a half-light radius that is drawn at random from all galaxies of the same F814W apparent magnitude in the observed COSMOS catalog. Thus the size-magnitude distribution of the simulated catalog will, by construction, exactly match

the COSMOS observations. The procedure does not reproduce any additional dependence of galaxy size upon type, color, or redshift using the COSMOS catalog. If needed, this can be implemented using a match between the simulated redshift and the COSMOS photometric redshift distribution.

2.1.4. Photometric Noise

A real survey has noise from the finite photon count and detector noise. Estimation of this noise is of course essential for forecasting survey performance. It may also be important for validation of the simulation against real data, since the noise can induce biases on number counts. Le Phare produces both noiseless magnitude and noisy magnitude for each chosen observation bandpass. The noisy magnitudes are randomly drawn inside a gaussian distribution centered around (m, err_m) . We define a reference couple (m^*, err^*) calculated from the survey characteristics and the error err_m at any magnitude m . **At magnitude $m < m^*$, the object noise is dominating and we assume that the magnitude error follows a power law of the adjustable form :**

$$err_m = 10^{(0.4(p+1)(m-m^*))} \quad (3)$$

At magnitude $m > m^*$, the sky noise is dominating and we assume the error on magnitude follows an exponential law :

$$err_m = err^* / 2.72 \cdot \exp(10^{(q(m-m^*))}) \quad (4)$$

(p, q) are the slopes for the power laws, both derived from the survey characteristic.

We will, however, use noiseless magnitudes for the validation tests in this paper, because the comparison surveys (e.g. the UDF) have high S/N in the regimes of comparison, and because the noise-induced biases are generally small.

2.2. CMC - The COSMOS Mock Catalog

The second simulated galaxy catalog is built directly from the observed COSMOS catalog of Capak et al. (2009) in prep. and Ilbert et al. (2009). We will refer to this simulation as the COSMOS mock Catalog (CMC).

2.2.1. The COSMOS catalog

The COSMOS photometric-redshift catalog Ilbert et al. (2009) was computed with 30 bands over $\sim 2\text{-deg}^2$ taken from Galax for UV bands, Subaru for the optical (U to z) and CFHT, UKIRT and Spitzer for the NIR bands. However, we restrict our mock catalog to the central square area of 1.38 deg^2 fully covered by HST/ACS images. The COSMOS-ACS catalog gives 592000 galaxies for an area of 1.38deg^2 . This is roughly a density of 120 galaxies by square arcmin down to $i^+ < 26.5$. In the COSMOS photometric-redshift catalog, 10% of this surface corresponds to masked areas because of bright stars that prevent multiband quality photometry with a deep photometry in the extended bright star halos. The effective area is thus in fact 1.24 deg^2 of unmasked region with a total number of 538000 simulated galaxies out to $i^+ < 26.5$ leading again to roughly a density of 120 gal/arcmin^2 . Point sources such as stars and X ray sources (mostly dominated by an AGN) were also removed from the mock catalog.

Based on a comparison between the photo-z and different spectroscopic sample like the zCOSMOS sample (bright down to $i_{med}^+ < 22.5$ with 4148 galaxies and faint down to

$i_{med}^+ < 24$ with 148 galaxies) and also the MIPS infrared selected sample bright and faint with 317 galaxies, Figure 7 and 8 of Ilbert et al. (2009), the COSMOS photo-z accuracy is $\sigma_{\Delta z/(1+z_s)} = 0.007$ at $i^+ < 22.5$ with a catastrophic rate below 1% see Figure 6 of Ilbert et al. (2009). At fainter magnitude and $z < 1.25$, the estimated accuracy is $\sigma_{\Delta z} = 0.02, 0.04, 0.07$ at $i^+ \sim 24, i^+ \sim 25, i^+ \sim 25.5$, respectively. The accuracy is degraded at $i^+ > 25.5$. The deep NIR and IRAC coverage enables the photo-z to be extended to $z \sim 2$ albeit with a lower accuracy ($\sigma_{\Delta z/(1+z_s)} = 0.06$ at $i_{AB}^+ \sim 24$) see Ilbert et al. (2009) for more details.

Despite the lower photo-z accuracy at $i^+ > 25.5$ and $z > 1.25$ and possible bias of faint AGN contribution, we used the full COSMOS catalog. Indeed, the photo-z accuracy is not crucial for the simulation. The COSMOS catalog is only used to obtain a representative population of galaxies in term of density and mix of galaxy types. Since the predicted apparent magnitudes are calculated from the best-fit templates, the photo-z accuracy has no impact on our ability to link the simulated redshift to the predicted colors. The only risk of including lower quality photo-z's is to degrade slightly the catalog representativity, possibly biasing the redshift distribution at $z > 1.25$.

2.2.2. The mock catalog construction

The principle of our simulation is to convert the observed properties of each COSMOS galaxy into simulated properties that can then be viewed using any possible instrument configuration. A photo-z and a best-fit template (including possible additional extinction) are associated with each galaxy of the COSMOS catalog.

The first step is to integrate the best-fit template (in the observer frame) through the instrument filter transmission curves to produce simulated magnitudes in the instrument filter set.

The second step is to apply random errors to the simulated magnitudes, based on the magnitude-error relations established in each filter (see Section 2.1.4).

Importantly, all the COSMOS measured properties are propagated to the simulated galaxies, for instance, the galaxy half-light radius as measured on the ACS images by Leauthaud et al. (2007).

This approach presents the following advantages:

- the simulated mix of galaxy populations is, by construction, representative of a real galaxy survey,
- additional quantities measured in COSMOS (like the galaxy size, UV luminosity, morphology, stellar masses, correlation in position) can be easily propagated to the simulated catalog.

The COSMOS mock catalog is limited to the range of magnitude space where the COSMOS imaging is complete ($i_{AB}^+ \sim 26.2$ for a 5σ detection, see Capak et al. (2007) and Capak et al. (2009) in prep.

2.2.3. Simulating emission lines

For each galaxy of the COSMOS mock catalog we have associated emission line fluxes. This feature is useful to predict the size and the depth of a spectroscopic redshift sample. We modeled the emission line fluxes ($\text{Ly}\alpha$, [OII], $\text{H}\beta$, [OIII] and $\text{H}\alpha$) of each galaxy as explained below.

We used the method described in Section 3.2 of Ilbert et al. (2009). Using the Kennicutt (1998) calibration, we first estimated the star formation rate (SFR) from the dust-corrected

UV rest-frame luminosity already measured for each COSMOS galaxy. The SFR can then be translated to an [OII] emission line flux using another calibration from Kennicutt (1998). We checked that the relation found between the [OII] fluxes and the UV luminosity is in good agreement with the VVDS data (see Fig.3 of Ilbert et al. (2009)) and still valid for different galaxy populations. For the other emission lines, we adopted intrinsic, unextincted flux ratios of $[OIII]/[OII] = 0.36$; $H\beta/[OII] = 0.28$; $H\alpha/[OII] = 1.77$ and $Ly\alpha/[OII] = 2$ (McCall et al. (1985), Moustakas et al. (2006), Mouhcine et al. (2005), Kennicutt (1998)). The approach of determining the $Ly\alpha$ line flux through its ratio with the OII emission line flux is perhaps not a good description but since the $Ly\alpha$ line becomes visible up to $z \sim 3$ for optical-NIR wavelength range it will not have a big impact on the studies about future optical-NIR dark energy surveys. Finally, we reduce each galaxy's line flux using the best-fit dust attenuation found with the template fitting procedure in the COSMOS photo-z catalog.

The same procedure can be applied to the GLFC since we can calculate the UV absolute luminosity the same way as for the CMC.

The COSMOS mock Catalog (CMC) has the advantage over the GLFC that it better preserves the relations between galaxy size and color (and presumably type and redshift). The CMC may also more accurately reproduce color distributions, since the population has not been reduced to three galaxy types as in the GLFC. The CMC is, however, limited by construction to the range of magnitude space where the COSMOS imaging is complete, whereas the GLFC can be extrapolated to fainter galaxies. Our validation tests below will compare the differences of these two simulation approaches. It is important to stress that all the following galaxy number densities correspond to mask corrected areas. Hence for real surveys, those numbers would have to be reduced by a factor of about ten % as observed in COSMOS field.

3. Validation

The aim of these mock catalogs is to predict the performance of future surveys such like JDEM and EUCLID. The depth of the foreseen surveys may be significantly fainter than the deepest existing spectroscopic and NIR imaging wide field surveys, so a comprehensive observational validation of the catalog is not yet possible especially in terms of NIR photometry and redshift distribution. We should, however, prove that the GLFC and CMC are consistent with existing data. For this validation, we will compare the galaxy counts, color distributions, redshift distributions, and emission-line distributions to a selection of the deepest available relevant survey data. The comparison data are taken from:

- The HST Ultra-Deep Field (UDF) catalog (Coe et al. 2006)² and included references covers 11.97 arcmin² in the 4 HST/ACS filters F435W, F606W, F775W and F850LP, referred to as B , V , i , and z bands, respectively and 5.76 arcmin² for the NICMOS filters F110W and F160W respectively the J and H-band. The UDF detects objects at 10σ for $z < 28.43$, $i < 29.01$ and $J < 28.3$, significantly fainter than the expected depth of any of the aforementioned proposed surveys. Due to the small area, the UDF is more sensitive to the cosmic variance, but it is useful for comparisons at faint magnitude.

- The GOODS (Great Observatories Origins Deep surveys) Giavalisco et al. (2004) v1.1 survey catalog³. The GOODS observations are split into northern and southern fields. Each field covers 160 arcmin² in the same $BViz$ filters as the UDF, and is 90% complete at $z \approx 26$.
- The GOODS-MUSIC (MUltiwavelength Southern Infrared Catalog) sample Grazian et al. (2006) has been constructed with public data of the GOODS-S field, NIR Spitzer data from IRAC instrument (3.6, 4.5, 5.8 and 8.0 μ m) and U-band data from the 2.2ESO and VLT-VIMOS covering 140 arcmin². This catalog is both z and K_s -selected and is 90% complete for $K_s < 23.8$ and $z < 26$.
- The VVDS-DEEP first epoch public release⁴ includes photometric data in BVRI VIRMOS-VLT bands over 0.49 deg² McCracken et al. (2003); a spectroscopic survey of targets with $I_{AB} < 24$ (Le Fèvre et al. 2005) with a sampling rate of 0.2 and a mean redshift of 0.86.
- The VVDS-DEEP NIR J and K_s photometry (Iovino et al. 2005) covers 170 arcmin² and is complete for $K_s < 22.5$. This sample contains the $BVri$ VIRMOS-VLT band and the JK_s ESO/NTT (New Technology Telescope) using the SOFI Near Infrared imaging camera.

A cut in the size-magnitude plane is applied to each dataset in order to remove stellar contamination, in case this has not already been done for published catalogs.

For each of the above listed surveys, both a CMC and a GLFC are constructed as described above, projecting both mock catalog onto the real surveys' filter sets.

3.1. Galaxy Counts

We compare the simulated galaxy counts (dN/dm) to those in the real catalogs listed above. The SEDs of each simulated galaxy is integrated over the bandpass of each real catalog.

In Figure 3 we compare the differential galaxy counts in the B , V , i , and z bands of the UDF and GOODS to those synthesized from the GLFC and CMC simulations. The UDF counts in the NIR are also compared to the simulations. Excellent agreement is seen between all sources for $21 < m < 26$, with some tendency for the UDF counts to be lower than other surveys. We attribute this to cosmic variance because of the very small UDF survey area. The difference between the simulated catalogs and the GOODS South is generally less than the difference between GOODS North and South ($\approx 15\%$). Note that the CMC becomes incomplete for $m > 26$ ($m > 25$ in the 1.6 μ m band), so will underestimate the galaxy yield in surveys deeper than these limits.

We also compare in Figure 3 the simulated K_s band counts to the GOODS-MUSIC and VVDS data. The K_s -band VVDS data of Iovino et al. (2005) are 90% complete at $I_{AB} = 25.5$. We see a very good agreement between the VVDS, GOODS-MUSIC and simulated catalogs at $K_s < 20$ and some discrepancies at fainter magnitudes. However, we measure a mean less than 17.9% difference between VVDS Iovino and CMC, 14.4% difference between VVDS Iovino and GLFC and 17.4% between GOODS-MUSIC and VVDS Iovino within the observation limits of these 2 surveys. We conclude that both simulated catalogs are well reproducing the K_s counts.

² <http://adcam.pha.jhu.edu/~coe/UDF/>

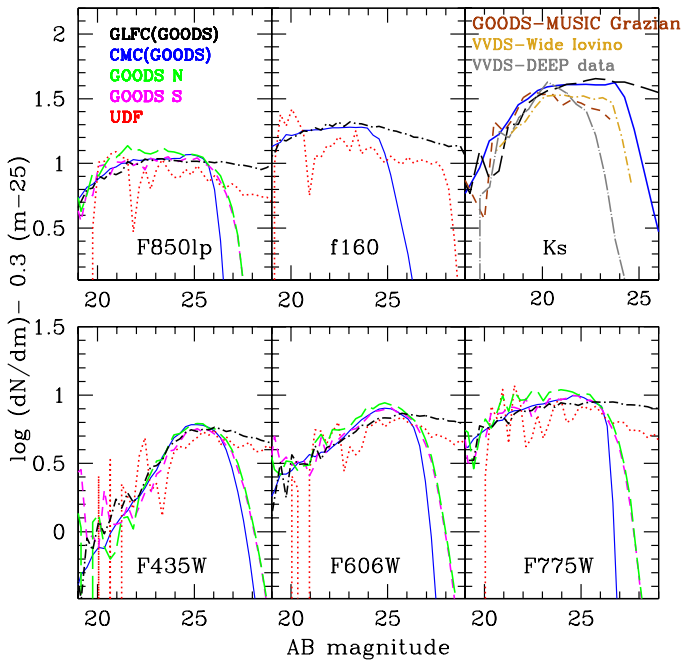


Fig. 3. Differential galaxy counts for F435W (B band), F775W (i band), F850LP (z band), F160W (H band) and the K_s band. The blue solid line is the COSMOS mock catalog (CMC) and the black dot-dashed line is the Le Phare simulation based on the GOODS LF (GLFC). The real observations are: the UDF (red dotted); GOODS North (long-dashed green) and South (dashed magenta). Note the excellent agreement between all simulations and real data where each is complete.

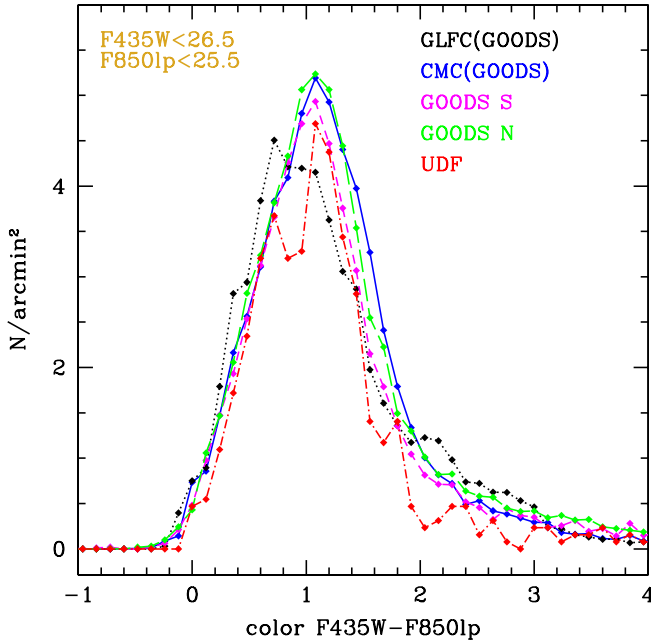


Fig. 4. Color histogram of F435W (B Band)-F850lp (z Band). The blue solid line is the simulation based on the COSMOS catalog (CMC) in GOODS filters and the black dotted line is the Le Phare simulation based on the GOODS LF and filters (GLFC). The real observations are: the UDF (dot-dashed red); GOODS North (long-dashed green) and South (dashed magenta). The indicated cut in S/N and magnitude are applied to F850LP (z Band) for each catalog.

3.2. Colors

Figure 4 compares the $B - z$ color distribution of the simulated catalogs to those of GOODS and UDF galaxies. The magnitude cuts in the B and z bands are taken following the COSMOS completeness in each of these bands. There is a good agreement in these optical wavelengths. The simulated catalogs have median and mean $B - z$ colors in agreement at a few percent with the UDF and GOODS catalogs (see table 3).

The UDF seems relatively deficient in the reddest galaxies, again perhaps a manifestation of cosmic variance, which is most severe for the highly-clustered red-sequence galaxies. **This is an expected result and is not an issue with the catalogues since the UDF may be under-dense due to its small survey area.**

Table 3. Mean and Median of the $B - z$ color distributions with the magnitude cuts of Figure 4 corresponding to the completeness of the CMC.

Catalogs	Mean	Median	survey area	mag limit
CMC(GOODS)	1.24	1.14	1.24 deg ²	$I \sim 26$
GLFC(GOODS)	1.2	1.05	0.1 deg ²	$R \sim 31$
GOODS-S	1.26	1.1	160 arcmin ²	$z \sim 26$
GOODS-N	1.3	1.13	160 arcmin ²	$z \sim 26$
UDF	1.16	1.06	11.97 arcmin ²	$z \sim 28.43$

Figure 5 compares simulated $B - K_s$ colors to those in the GOODS-MUSIC and VVDS-DEEP catalog. The color distributions in NIR agree well inside the completeness limits imposed by the different surveys, the CMC $z < 25.5$ and $B < 26.5$ and the GOODS-MUSIC survey $K_s < 22.5$. The GOODS-MUSIC data have lower $B - K_s$ counts which is explained by the number count difference at $K_s > 20$ in the K_s -band between both simulated catalogs and the Grazian count see Figure 3. However, the mean and median are in good agreement with this latter. The agreement is much better in Figure 5b between the CMC, GLFC and VVDS-DEEP data.

3.3. Redshifts

Comparison of the simulated redshift distributions to real data is likely less accurate than colors or magnitudes, since real redshift surveys are much shallower and have significant incompleteness. Nonetheless we plot in Figure 6 the median redshift vs I -band magnitude for the CMC and GLFC catalogs and the VVDS survey.

The redshift quartiles of the CMC agree very well with the VVDS spectroscopic redshift distribution to the $I = 24$ limit of the latter. The GLFC seems to have a lower median redshift, probably due to the GOODS LF used to produce the catalog. The mean difference of the median redshift is 0.02 and respectively 0.07 for the CMC and GLFC catalogs. We conclude not surprisingly that the CMC is probably a better representation of the magnitude-redshift distribution, and is as accurate as current data can validate. Figure 7 plots median $B - i$ color vs redshift for the simulated catalogs CMC and GLFC and for the VVDS-DEEP. All catalogs have been restricted to $I < 24$, the domain of the VVDS-DEEP redshift survey. The colors agree to 0.1–0.2 mag until $z \sim 2$. Above this redshift the VVDS survey is likely highly incomplete in this regime, even for blue galaxies, as no

³ <http://archive.stsci.edu/prepds/goods/>

⁴ <http://cencos.oamp.fr/>

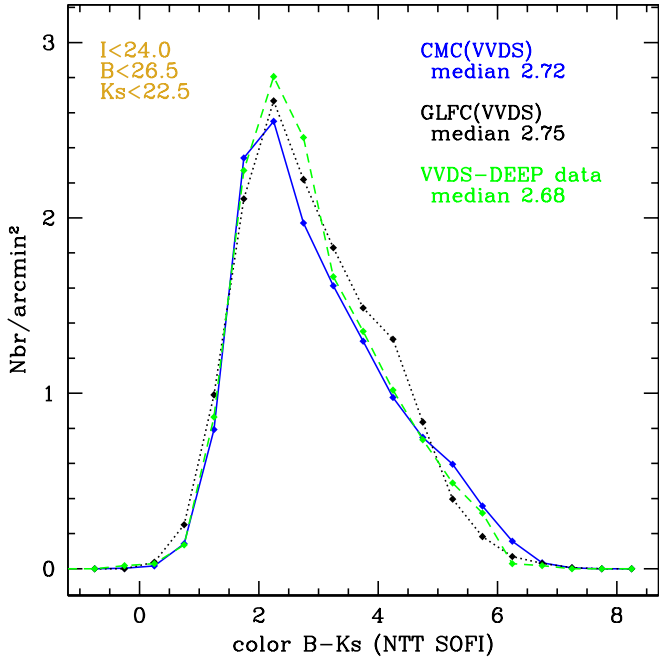
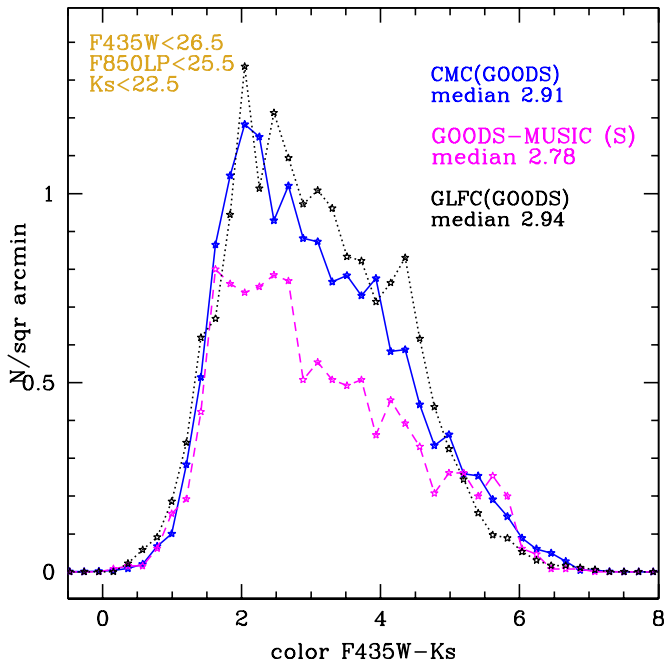


Fig. 5. Color histogram of F435W (B Band)- K_s . The blue solid line is the COSMOS mock catalog (CMC) and the black dotted line is the Le Phare simulation based on the GOODS LF (GLFC). The observational data are the GOODS-MUSIC (top panel) catalog in dashed magenta and VVDS (bottom panel) catalog in dashed green. We choose to cut at 22.5 AB mag in the K_s Band due to the area variability of the GOODS-MUSIC sample above this magnitude and the VVDS completeness.

strong emission lines are available in the VVDS spectral wavelength range and due to the $I = 24$ magnitude cut see Figure 6 for the median redshift and quartiles of the distribution.

We compare the redshift distributions Figure 8 for different magnitude cuts.

The CMC and the VVDS-DEEP catalog show very good agreement. This figure shows that both mock catalogs are well reproducing the number density inside the VVDS volume : ($0 <$

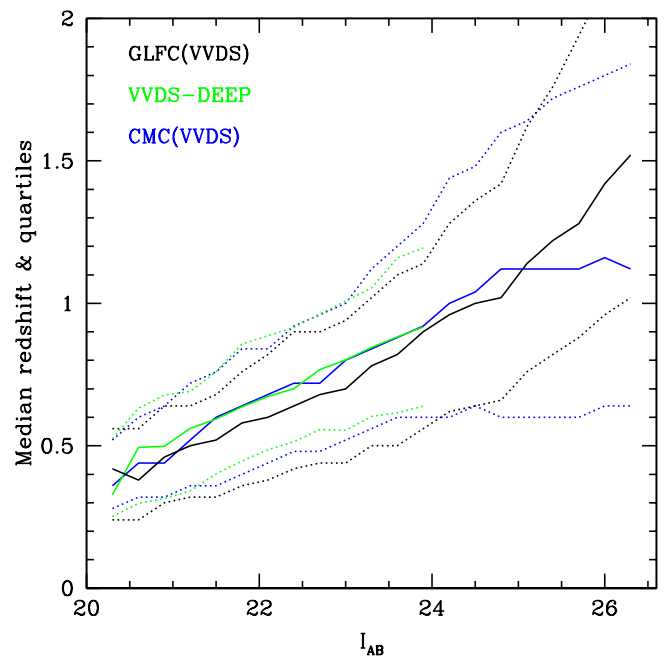


Fig. 6. Median redshift distribution function of the magnitude i Band VVDS magnitude. The continuous lines are the median redshift and the dotted lines represents the quartiles. The blue line is the simulation based on the COSMOS catalog (CMC) in VVDS filters and the black line is the Le Phare simulation based on the GOODS LF in VVDS filters (GLFC). The real observation is the VVDS-DEEP catalog (green). The indicated cut in S/N is applied to I VVDS Band. We note the very good agreement between the median redshift of the COSMOS and VVDS-DEEP catalogs.

$z < 1.5$ and $I < 24$) and agree at higher magnitude and redshift. The GLFC is based on the GOODS luminosity function Dahlen et al. (2005) which has equivalent depth to the VVDS galaxy sample. However, in looking at Figure 6, the VVDS magnitude-redshift distribution seems in better agreement with the CMC than the GLFC.

3.4. Emission-Line Strength

Future dark energy surveys need large spectroscopic redshift samples to calibrating photometric redshifts, measuring accurately the BAO and for other probes using spectroscopic samples of galaxies. Thus, this is crucial to have realistic emission lines allowing to make predictions on the success rate, depth, and size of spectroscopic samples that we will need to answer fundamental questions which justify the future surveys we are planning. Although, the CMC does not reproduce absorption lines, it simulates emissions lines for all galaxies in the catalogue which allows a first estimation of spectroscopic survey capacities. The validation of the emission line strength can be found in Figure 3 of Ilbert et al. (2009). This figure shows the relation between the OII flux and the rest-frame UV luminosity predicted by Kennicutt (1998) :

$$\log[OII] = -0.4M_{UV} + 10.57 - \frac{DM(z)}{2.5} \quad (5)$$

It shows very good agreement between VVDS data from Lamareille et al. (2008) and the simulated emission lines strength extrapolated from the photometric redshift best fit tem-

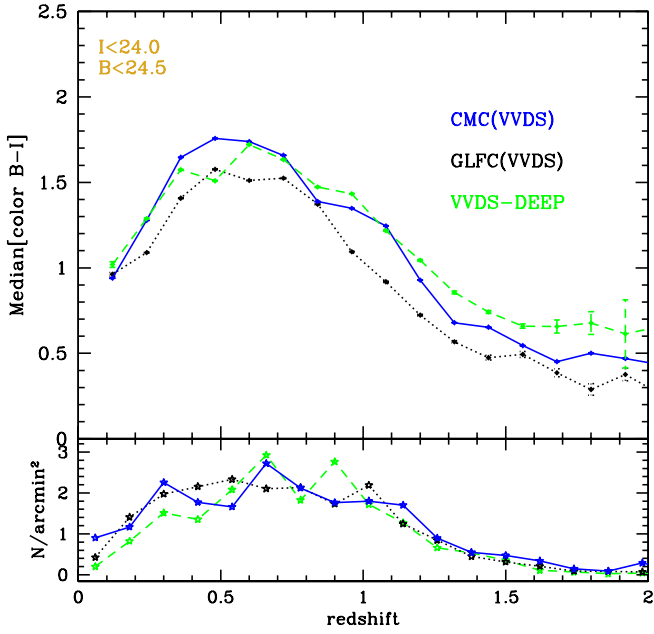


Fig. 7. Median color of B-i VVDS band function of the redshift. The blue solid line is the simulation based on the COSMOS catalog (CMC) in VVDS filters and the black dotted line is the Le Phare simulation based on the GOODS LF in VVDS filters (GLFC). The real observation is the VVDS-DEEP catalog in dashed green. The indicated cut in S/N is applied to i Band VVDS and the i Band magnitude cut is the completeness limits of the VVDS-DEEP catalog. The error bars are drawn from the root of number of objects. There is a good agreement between the VVDS-DEEP and COSMOS catalog as well as the GLFC until a redshift around 1.8.

plate between $0.4 < z < 1.4$ where the OII emission line can be measured.

The histograms shown Figure 9 are the emission line ratios of the CMC compared with those of VVDS. The attenuation causes a spread on the emission line ratios but we had to add a gaussian dispersion to fit the VVDS emission line spread. Knowing that r is a number randomly drawn from a gaussian law $(\mu, \sigma^2) = (0, 1)$, we define the new fluxes as :

$$H\alpha = H\alpha(1 + |r/4|) \quad (6)$$

$$H\beta = H\beta(1 + |r/2|) \quad (7)$$

$$[OIII]_{4959} = [OIII]_{4959}(1 + |1.2r|) \quad (8)$$

$$[OIII]_{5007} = [OIII]_{5007}(1 + |r|) \quad (9)$$

The spectral wavelength range of VVDS spans from 0.55 to $0.94\mu\text{m}$ (Le Fèvre et al. 2005) making the $[OII]$ line visible from redshift 0.5 to 1.5 and the $H\alpha$ line visible from redshift 0 to 0.5. Thus we choose to evaluate the validity of the $H\alpha$ fluxes using the ratio $H\alpha/H\beta$, known as the Balmer decrement and having a value ~ 2.9 . All CMC ratio spread fits well those of VVDS.

For a further validation of the CMC emission lines we choose to reproduce the spectroscopic success rate (SSR) of the VVDS survey. To realise the CMC(VVDS) SSR we have extrapolated the flux sensitivity of the VVDS survey in fonction of wavelength for several signal-to-noise ratio based on the $[OII]$ emission lines. Using these sensitivities and the CMC emission line catalog we derive the simulated SSR for the VVDS survey in order to validate the emission line model of the CMC catalog (Figures 10 and 11). Figures 10 shows the SSR for the

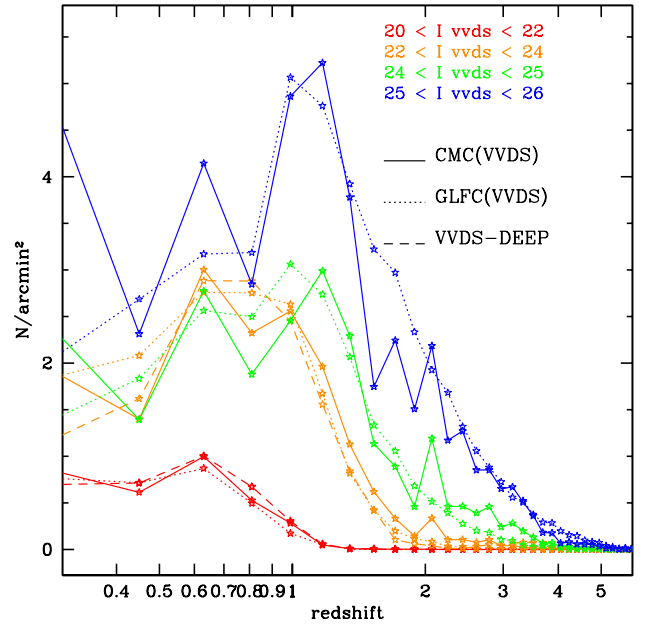


Fig. 8. Redshift distribution. The blue solid line is the simulation based on the COSMOS catalog (CMC) in VVDS filters and the black dotted line is the Le Phare simulation based on the GOODS LF in VVDS filters (GLFC). The real observation is the VVDS-DEEP catalog in dashed green. The indicated cut in S/N is applied to I VVDS Band and the i Band magnitude cut is the completeness limits of the VVDS-DEEP catalog. There is a very good agreement between the VVDS-DEEP, COSMOS and GLFC redshift distribution.

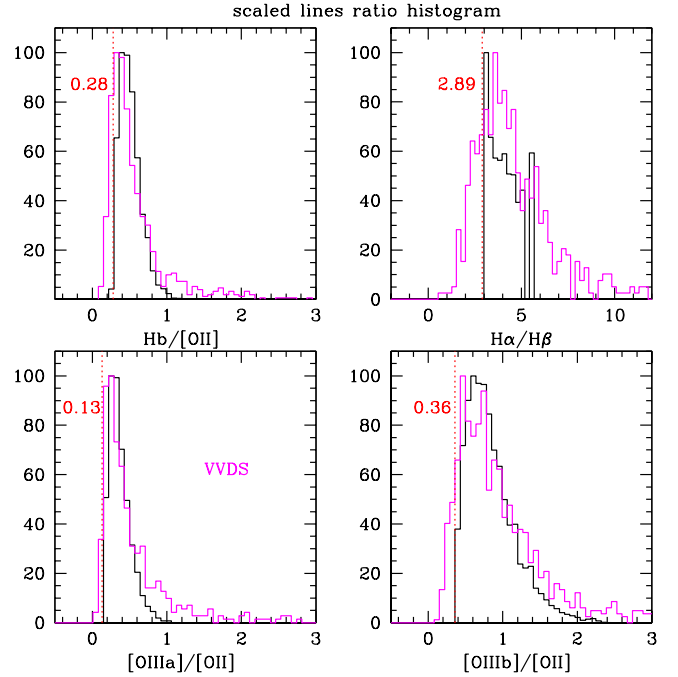


Fig. 9. Emission line ratios. The magenta histograms are the VVDS survey and the black histograms the CMC. The red dotted line is the value of the theoretical emission line ratios.

emission lines of the CMC catalog compared to those of the VVDS in fonction of redshift (top panel) and magnitude (bottom panel). The strong emission lines, $H\alpha$ and OII, are in very good agreement with the VVDS both in magnitude and redshift

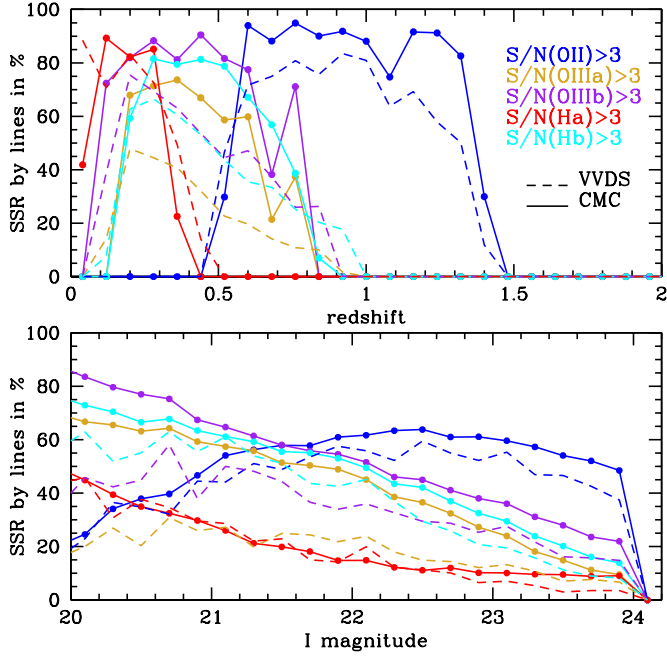


Fig. 10. Comparison of the lines Spectroscopic Success Rate (SSR) of the VVDS survey with the simulated lines VVDS SSR using the CMC emission lines. **Top panel** shows the SSR of emission lines as a function of redshift, dashed lines for the VVDS survey and solid lines for the CMC. The blue lines are for the OII lines, red for H α , cyan for H β , gold for OIIIa at 4959Å and purple for OIII at 5007Å. **Bottom panel** shows the same as the top panel as a function of magnitude.

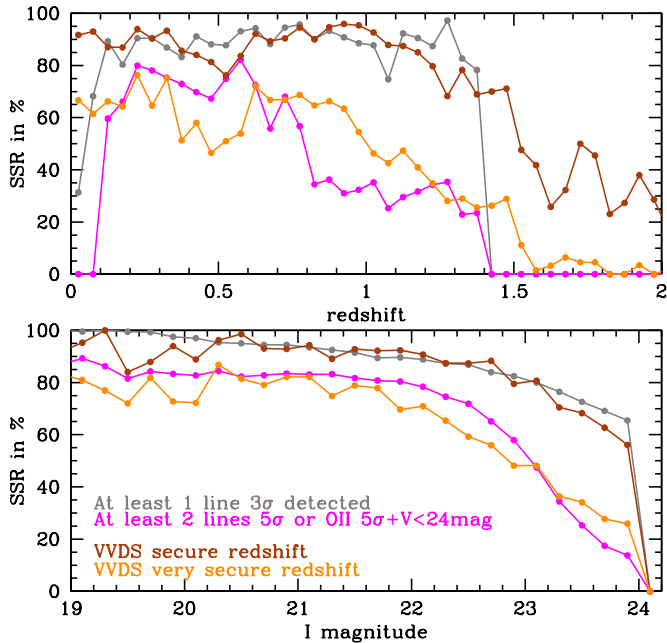


Fig. 11. Comparison of the Spectroscopic Success Rate (SSR) of the VVDS survey with the simulated VVDS SSR using the CMC emission lines. **Top panel** shows the VVDS SSR for secure redshift (brown lines) and very secure redshift (orange line) as a function of redshift compared to the CMC emission lines 3 σ VVDS flux detection (grey lines) and 2 lines at 5 σ detection or OII at 5 σ detection with $V < 24$. **Bottom panel** shows the same as the bottom panel as a function of magnitude.

space. However weaker emission lines have a discrepancy from 10 to 20 % with the VVDS emission lines at low magnitudes especially for the [OIII] lines at 4959Å and 5007Å but it agrees very well at magnitudes $I > 21$. Figure 11 compare the overall SSR predictions of the CMC with the VVDS secure and very secure redshifts. We see that the VVDS secure redshifts success rate are very close to the 3 σ detection line of the CMC catalog. In the same way, the VVDS very secure redshift success rate agrees very well with the 2 lines detection at 5 σ including galaxies with $V < 24$ which corresponds to a detection of the continuum in the VVDS spectra with a $S/N > 10$ in the blue part of the spectrum (which is free of strong sky emission lines). The differences mainly comes from the redshifts effectively obtained using absorption lines for which the shape of the continuum altogether does not match exactly with our ad-hoc V-band magnitude criterion. Although, the CMC does not simulate the absorption lines, we can say that the CMC emission line shows a good agreement both in redshift and magnitude with the VVDS spectroscopic survey. These results makes us confident in using the CMC catalog as a tool to predict the SSR of future wide field spectroscopic surveys.

4. Discussion

Different cosmological tests have been proposed to probe the geometry and growth of structures in order to shade new light on the nature of dark energy. The best approach is certainly to combine different probes to reduce the errors and better understand the systematics. However, each probe has its own requirement and it is a technical and scientific challenge to design a telescope optimised for more than one cosmological probe. Nonetheless, the goal of future dark energy programs should find a survey strategies that will lead to the best combination efficiency of different probes.

Having a realistic description of galaxy properties in our Universe is key to properly forecast what future deep and wide surveys can achieve for a given survey configuration. In this section, we start a discussion about WL requirements with the shape measurement and the photo-z calibration survey (PZCS) which is required in order to use weak lensing tomography to constrain Dark Energy parameters that we aim to combine with BAO estimations of the Dark Energy parameters.

Thus, we will discuss two important aspects of these future dark energy mission: (i) the impact of galaxy size in terms of shape measurement for weak lensing depending on the PSF size (ii) the different typical WL and BAO survey configuration we have tested using our mock catalogues and (iii) their expected spectroscopic success rate.

Note that we are not conducting here any optimisation of such space mission and its survey strategy. We are just putting in place some of the needed tool necessary for such optimisation.

4.1. Galaxy-sizes

A comparison of the simulated galaxy-size distribution to observational data is not particularly useful. Indeed the simulated catalogs agree, by construction, with the size distribution measured in the COSMOS ACS imaging survey Koekemoer et al. (2007), Leauthaud et al. (2007). No other survey capable of resolving faint galaxies approaches the size of the COSMOS/ACS data. In

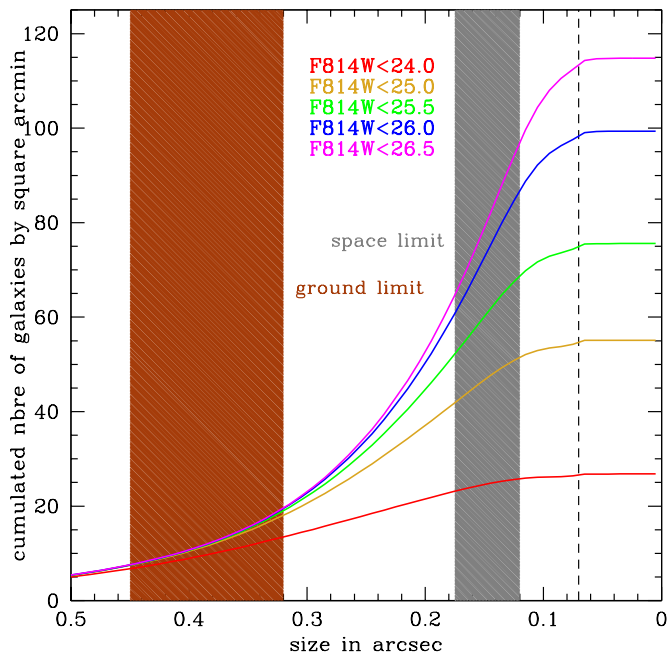


Fig. 12. Cumulated Half-light radius distribution by bins of magnitude. The brown area is the PSF size of ground-based telescope, the grey area is an estimation of the PSF size of future dark energy mission and the black dashed line is the measured PSF size of the COSMOS space survey (Leauthaud et al. 2007).

Figure 12 we show the cumulated half-light radius distribution for the COSMOS data.

The brown area corresponds to the typical PSF size of ground-based telescopes. It shows that we can only resolve and measure galaxy shapes (those galaxies with a size larger than the PSF size) for about 15gal/arcmin² (or up to 20gal/arcmin² in case of excellent seeing) as soon as a depth of $I \sim 25$ is reached. Going deeper than $I = 25$ will not help to raise this number density as fainter galaxies are smaller than the PSF, thus making a shape measurement impossible.

The grey area corresponds to the PSF size expected with future space Dark Energy mission; the exact value of the PSF size depends on the telescope diameter and the chosen pixel scale (here we assume a telescope diameter of $\sim 1.5 - 1.8$ meter). Interestingly, with this small PSF size, the number density of resolved galaxies does increase as a function of the depth of the survey. Beyond $I = 26$ the increase in number density is however smaller, suggesting that there is a limited gain to go much deeper than $I = 26$ except may be for telescope designs with the smallest PSF size. With a depth of $I \sim 25.5 - 26$ the number density of resolved galaxies in the foreseen space surveys is about $3\times$ larger than what ground-survey can achieve.

Contrary to the ground case, the performance of a space survey in terms of galaxy number density critically depends on the characteristic of the survey in terms of depth and image resolution. The black dashed vertical line correspond to the PSF size of the ACS/HST camera as measured in the COSMOS survey Leauthaud et al. (2007). The COSMOS survey reach a number density of resolved galaxies of ~ 110 gal/arcmin² down to $I \sim 26.5$. It is important to recognized however that not all these galaxies could be used in the COSMOS 3D weak lensing analysis as explained in Leauthaud et al (2007). For a fraction of these galaxies there was no counterpart in the ground-based catalogue because of masking of the data. For the remaining galaxies, it

was not always possible to determine securely the shape or the redshift thus decreasing further the number of usable galaxies to roughly 40gal/arcmin².

Cosmological weak lensing survey aim to maximize the number of resolved galaxies that can be used for weak lensing tomography. As shown by Amara & Réfrégier (2007) it is more efficient to conduct a wider survey than a deeper survey as the galaxy number increase is larger for a given exposure time by going wide than by going deep. However the sky brightness and the variable star density is limiting this prescription to typically 10000 to 15000 deg², a quarter of the sky area.

4.2. BAO and WL spectroscopic survey requirements

We investigate here three types of spectroscopic redshift survey (see Figure 13 and Table 4) whose characteristics correspond to typical requirements for the BAO and WL probes.

(i) BAO aims to measure the baryon acoustic oscillation peak of the 2-pt correlation function as a measure of a standard ruler. It requires a large survey area to reduce the statistical noise (Glazebrook & Blake 2005; Blake & Glazebrook 2003) and an accurate redshift for each galaxy, typically using spectroscopic techniques to reach a higher accuracy. There are studies about using photometric redshift instead of spectroscopic redshift but it then needs a larger area (typically a few times larger in area) due to the precision loss of the scales along the line of sight to reach the same dark energy figure of merit (FOM) Glazebrook & Blake (2005). Following this last paper, we develop a WIDE near infrared (1.0 to 1.7 micron) spectroscopic survey reaching a 3σ sensitivity of 1×10^{-16} ergs cm⁻² s⁻¹ at 1.2 μ m (this can be achieved with an efficient slitless spectrograph using a 1.5m telescope, 0.28"/pixel, R \sim 500 and an exposure time of 1200 sec) and covering a large area on the sky to maximise the dark energy FOM.

(ii) The weak-lensing tomographic analysis is likely the most efficient lensing method to estimate the Dark energy parameters (Massey et al. 2007), (Amara & Réfrégier 2007). This method probes the growth of structures but needs to have accurate redshifts to place the background sources at their correct location. To achieve this measurement, it is essential to determine with the best accuracy (and minimal biases) the photometric redshift (photo-z) of all the galaxies to be used in the weak lensing tomography. Ma & Bernstein (2008) have shown that a high accuracy photo-z is needed to avoid any bias on the Dark Energy parameter estimation. The only way to reach high accuracy photo-z is to plan a spectroscopic redshift survey to calibrate the photo-z templates similarly as shown in Ilbert et al. (2006). Ideally, the photo-z calibration survey (PZCS) would reach the same magnitude and redshift depth as the WL photometric survey. However, this goal will likely be difficult to achieve and the CMC may help to foresee the best spectroscopic surveys through its emission line catalog usefully complementing the photometric catalog. Thus, we design a DEEP-visible-NIR survey (0.6 to 1.7 microns) for weak-lensing reaching a 3σ flux sensitivity of 5.10^{-18} ergs cm⁻² s⁻¹ at 1.2 μ m (this can be achieved with an efficient slitless spectrograph using a 1.5m telescope, 0.28"/pixel, R \sim 250 and an exposure time of 240 ksec \sim 67 hours) in order to have a large number of spectroscopic redshift allowing a full calibration of the photometric redshift for a wide range in redshift and magnitude.

(iii) We also design a DEEP-NIR survey having the same characteristics that the DEEP-visible-NIR survey but covering only the NIR part (1.0 to 1.7 micron); focussing on the low IR background of space observation). Our goal here is to evaluate the importance of having a spectroscopic contribution in the visible wavelength to reach a high completeness.

4.3. SSR prediction

In the following sections we will give the basics of photo-z calibrations survey studies based on spectroscopic success rate as a function of redshift and magnitude. A more thorough analysis will be developed in more details in a forthcoming paper (Jouvel et al 2009 in prep).

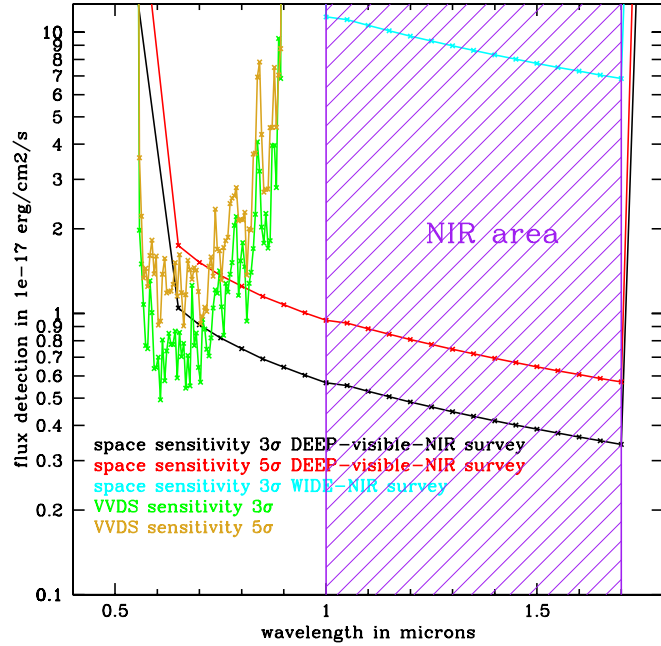


Fig. 13. Flux sensitivities for VVDS-DEEP survey (~ 10 sec exposure on a 8m ground-based telescope with a spectroscopic resolution of $R=250$) at 3σ in green and 5σ in gold as a function of wavelength compared to space sensitivities for (i) a WIDE space near infrared survey reaching a 3σ flux sensitivity of 10^{-16} erg/s/cm 2 at $1.2\mu\text{m}$ [The cyan curve for the WIDE NIR survey sensitivity at 3σ .]; (ii) a DEEP-visible-NIR survey reaching a 3σ flux sensitivity of 5.10^{-18} erg/s/cm 2 at $1.2\mu\text{m}$. [The black curve for the DEEP-visible-NIR space survey sensitivity at 3σ and the red curve at 5σ .] We will also consider the DEEP-NIR survey which is identical to the DEEP-visible-NIR but limited to the NIR domain [the purple area].

4.3.1. SSR for the WIDE survey

The wide survey would aim to cover a large fraction of the sky (10,000 deg 2 or more) in order to probe the large scale distribution of galaxies aiming in particular to measure the baryon acoustic oscillation with a great accuracy in the redshift range $0.5 < z \lesssim 1.5$ (or up to $z \sim 2$ providing the telescope and instrument is sensitive up to $2\mu\text{m}$). Our SSR prediction, shows that such survey could easily measure the redshift of more than 4 galaxy/arcmin 2 hence providing the redshift measurement of more than ~ 100 million galaxies for a survey covering 10,000 deg 2 . The redshift identification is essentially based on the $H\alpha$

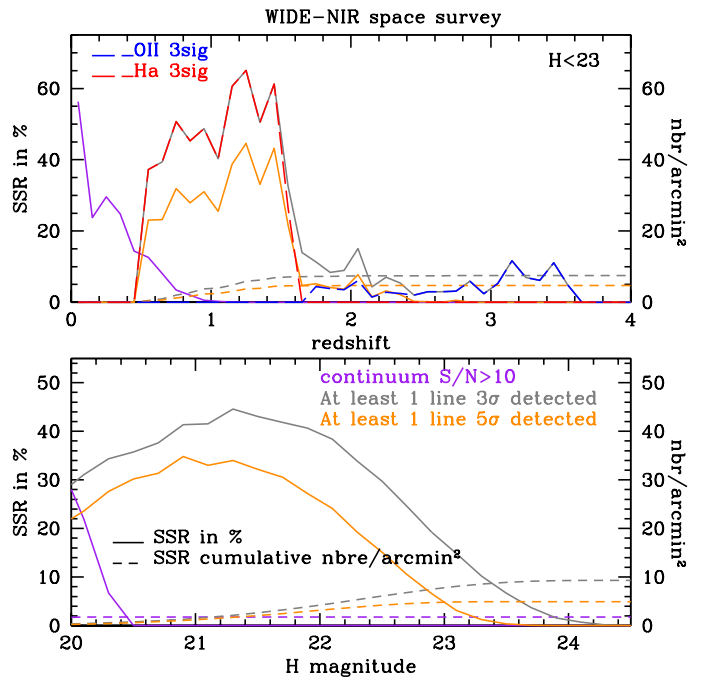


Fig. 14. WIDE NIR space survey SSR **Top panel** : SSR as a function of redshift limited to galaxies with $H < 23.5$. The long-dashed red curve is the SSR of the $H\alpha$ 3σ detection line and the long-dashed blue curve the SSR of the [OII] 3σ detection line. **Bottom panel** : SSR as a function of magnitude. **Both panels** : the orange lines shows the SSR using a 1 at 5σ criterion, the grey curve using a 1 line at 3σ criterion, and the purple using a continuum $S/N > 10$ criterion. The solid curves are a percentage with the total number of objects and the dashed for a cumulative number of objects by arcmin 2 . The purple curve shows the SSR.

line detection thus essentially targeting star-forming galaxies with $H \lesssim 22.5$. The SSR clearly shows that such survey is far from being complete as the spectroscopic success rate is generally below 40% for any magnitude and redshift (for a 5σ line detection). **Indeed, there is no faint galaxies spectroscopically found, especially in the redshift range which has the strongest need of photometric redshift calibration : $0 < z < 0.5$ and $z > 1.5$. We also note the severe galaxy type incompleteness even from early to late type galaxies, see Table 4.** Thus, such wide survey *can not be used* to calibrate properly any photometric redshift catalogue.

4.3.2. SSR for the DEEP survey

Figures 15 and 16 show the SSR prediction for future dark energy surveys which are planning to do infrared only (DEEP-NIR survey), and visible+infrared spectroscopy (DEEP-visible-NIR survey) from space. Figure 13 show the grism flux sensitivity we use in our analysis.

We assume here that the visible spectroscopy spans $0.6-1\mu\text{m}$ see Figure 13. Because of the limited wavelength coverage, the $H\alpha$ is the only strong emission line visible for galaxies at low redshift ($z < 0.5$). This explains that the detection criterion based on 2 lines, does not cover the low redshift range as shown in the top panel of Figure 15. This is also seen in the bottom panel of Figure 15 where there is a lower SSR for bright galaxies. However, for these low redshift ($z < 0.5$) galaxies, about 30% have a strong continuum with $S/N > 10$. For these bright galaxies, we should be able to accurately measure a redshift using either

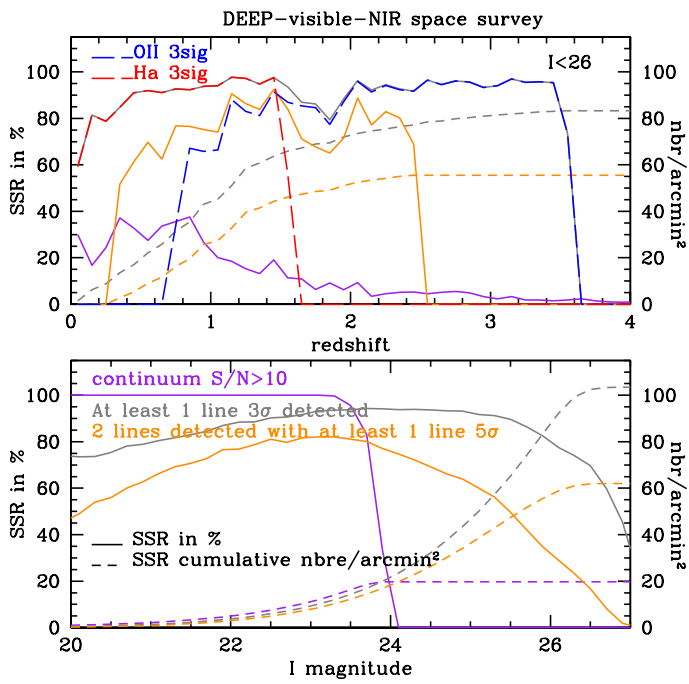


Fig. 15. DEEP-visible-NIR space survey SSR. **Top panel** : SSR as a function of redshift. The long-dashed red curve is the SSR of the H α detection line and the long-dashed blue curve the SSR of the [OII] detection line. **Bottom panel** : SSR as a function of magnitude. **Both panels** : the orange lines shows the SSR using a 2 lines with at least 1 at 5 σ criterion, the grey curve using a 1 line at 3 σ criterion, and the purple using a continuum S/N > 10 criterion. The solid curves are a percentage with the total number of objects and the dashed for a cumulative number of objects by arcmin². The purple curve shows the SSR.

the H α line detection, absorption lines and the shape of the continuum which will be useful for photometric redshift calibration.

If only the NIR spectroscopy is conducted from space, the survey will only reach ~ 35 galaxy per arcmin² and a maximal SSR of at best 40% for $I \sim 24$. Using DEEP-NIR spectroscopic survey would help to calibrate spectra at $0.8 < z < 2.5$ but would be less efficient below $z < 0.8$. There will be a strong need to conduct the visible spectroscopy to achieve a complete census of the redshift distribution.

Using the DEEP-visible-NIR survey, we should be able to measure a very secure redshift (2 lines detected at more than 3 σ with at least 1 emission line at 5 σ) for about 60 galaxy per arcmin² to $I < 26$ and $z \lesssim 2.5$ with a SSR reaching 80% at best for $I \sim 24$. With this density of sources, a survey of 1 square degree will provide 220000 spectra. Note however, that these numbers do not take into account the crowding of galaxy spectra which is likely a strong limiting factor above $I \sim 24$. There are ways to minimize the impact of crowding, for example by conducting the slit-less spectroscopic survey using different orientations, or by using masks to block some of the light (thus limiting the sky background and reducing the number of overlapping spectra). These alternatives will be discussed in a forthcoming paper Zoubian et al. 2009 in prep. . Note also that the visible part of the spectroscopy might be conducted with a dedicated ground-based spectrograph with high-multiplexing (this can probably be more efficient specially for $\lambda < 0.75\mu\text{m}$ where the sky emission lines are less numerous than in the redder part of the spectrum).

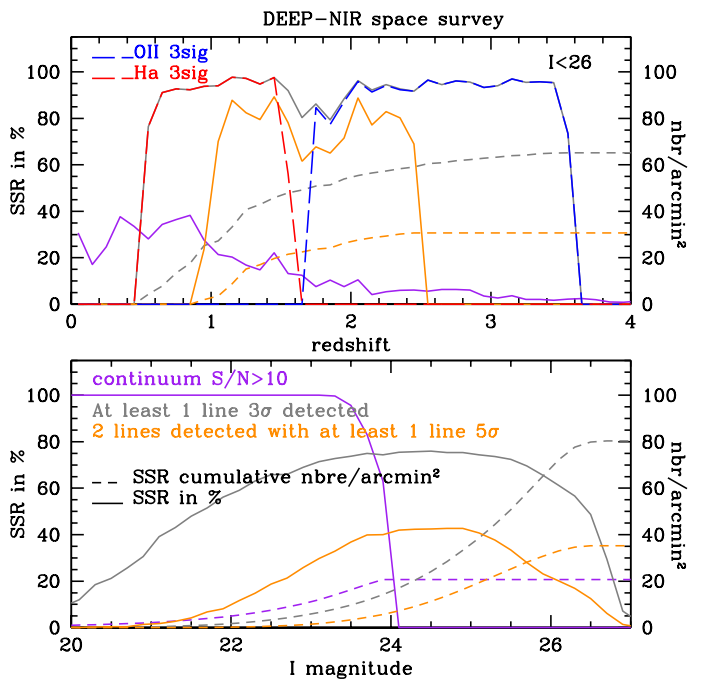


Fig. 16. DEEP-NIR only space survey SSR. **Top panel** : SSR as a function of redshift. The long-dashed red curve is the SSR of the H α detection line and the long-dashed blue curve the SSR of the [OII] detection line. **Bottom panel** : SSR as a function of magnitude. **Both panels** : the orange lines shows the SSR using a 2 lines with at least 1 at 5 σ criterion, the grey curve using a 1 line at 3 σ criterion, and the purple using a continuum S/N > 10 criterion. The solid curves are a percentage with the total number of objects and the dashed for a cumulative number of objects by arcmin². The purple curve shows the SSR.

Table 4. Characteristics of the three surveys discussed in the text, assuming an efficient 1.5m space telescope with an obscuration of 0.6m and a total telescope throughput of 92% using a survey efficiency of 75%. The % [1line3 σ] Ell represent the percentage of Elliptical galaxies spectroscopically found using a criterium of 1 line detected at 3 σ compared to the total population of Elliptical galaxies. With the same criterium, we define the percentage of Sac for early spiral galaxies, Sdm for late spiral galaxies, and SB for starburst galaxies.

	DEEP-vis-NIR	DEEP-NIR	WIDE-NIR
probe	WL	WL	BAO
T_{obs}	240ksec	240ksec	1200sec
λ in μm	0.6-1.7	1-1.7	1-1.7
3σ at 1.2 μm	$5 \cdot 10^{-18}$	$5 \cdot 10^{-18}$	$1 \cdot 10^{-16}$
area needed	10deg ²	10deg ²	20000deg ²
mission time	0.2yrs	0.2yrs	2yrs
nbr density (5 σ)	60	35	5
		ergs cm ⁻² sec ⁻¹	
		FOV of 0.5deg ²	
		gal/arcmin ²	
z[1line3 σ]	$0 < z < 3.5$	$0.5 < z < 3.5$	$0.5 < z < 1.5$
m_{lim} [1line3 σ]	$I \sim 27$	$I \sim 26.5$	$H \sim 22$
%[1line3 σ] Ell	40	27	0
%[1line3 σ] Sac	60	51	1
%[1line3 σ] Sdm	77	63	10
%[1line3 σ] SB	95	74	45

5. Conclusion

We have produced simulated deep galaxy catalogs by two different techniques: one starts with redshift-dependent Schechter

luminosity functions for three galaxy types for $0 < z < 6$, extrapolating the LFs derived from GOODS data by Dahlen et al. (2005) (the GLFC). The other has galaxies with redshifts and SEDs taken as the best photo- z fits to multiwavelength observations of the COSMOS field (the CMC). Both adopt galaxy size distributions from the COSMOS HST imaging and we assign emission line strengths using a recipe in agreement with the VVDS-DEEP data.

Both simulated catalogs do an excellent job of reproducing the dN/dm data ($< 20\%$ discrepancies) and color distributions (0.1–0.2 mag median color discrepancies) of galaxies observed in bands from 0.4 to 2.2 μm using a comparison with the GOODS and UDF surveys. The CMC provides an excellent match to the redshift-magnitude and redshift-color distributions for $I < 24$ galaxies in the VVDS spectroscopic redshift survey.

These simulated catalogs thus pass all our validation tests for use in forecasting the galaxy “yields” of future visible/NIR imaging surveys, as long as we restrict our analysis to the $I < 25.5$ –26 galaxies for which the COSMOS HST imaging is highly complete. These simulated catalogs provide a conservative estimate of the yield for surveys that go deeper in the visible, or reach > 24 in the NIR, because they miss faint or red galaxies that do not make the I -band cut.

The GLFC has the potential to forecast deeper surveys than the CMC, but only if we are ready to extrapolate the luminosity functions to fainter magnitudes, which is probably OK in the visible bands, but it may be more strongly limited in the near-infrared bands.

In the CMC, the galaxy sizes are directly coming from the HST/ACS measurement and give us the opportunity to evaluate the difference in terms of possible shape measurement for a ground-based and space based telescope. We showed that a ground based WL survey is limited to use only the resolved galaxy and thus it is basically independent of the survey depth for $I > 25$ (as most of $I > 25$ galaxies are smaller than the ground based seeing disk). For a space based survey the number of resolved galaxies is not only dependent of the PSF but also the depth of the survey.

Moreover we have also used the CMC and the emission line model to compare the spectroscopic success rate observed by the VVDS and the one we can predicted based on the CMC line flux. In general we obtain a good agreement between the observed success rate and the CMC prediction.

We have then used the emission line model to explore what will be the yield in terms of redshift measurement for 2 types of surveys: (i) a WIDE survey motivated by measuring BAO, and (ii) a deep survey motivated to calibrate the photometric-redshift. We found that the WIDE survey reaches a density of 4gal/arcmin² for galaxies $H \lesssim 22.5$ in a redshift range of $0.5 < z < 1.5$ mainly detected using the $H\alpha$ emission line. Furthermore, in a weak-lensing perspective, a DEEP survey both visible and NIR is needed to conduct the photometric redshift calibration of galaxies (PZCS) to be used in a weak-lensing measurement covering the full magnitude and redshift range. Indeed such survey reaches a density of 60 gal/arcmin² for very secure redshift down to $I \sim 25.5$ with a high completeness of $\sim 80\%$. We note that the visible part of the spectroscopic survey can be done from the ground however above $\lambda \sim 0.75\mu\text{m}$ as we can see Figure 13 a space based survey is likely to be much more efficient than a ground based survey.

We have thus demonstrated here how useful realistic simulated catalogue are for designing future DE space mission. We will investigate more precisely the details of the WL optimisa-

tion survey strategy in a forthcoming paper (Jouvel et al. 2009, in prep.).

Acknowledgements. We acknowledge useful discussion with the members of the COSMOS and SNAP collaborations. Stephanie Jouvel thanks CNES and CNRS for her PhD studentship. Jean-Paul Kneib thanks CNRS for support. Gary Bernstein is supported by grant AST-0607667 from the National Science Foundation, Department of Energy grant DOE-DE-FG02-95ER40893, and NASA grant BEFS-04-0014-0018.

References

- Amara, A. & Réfrégier, A. 2007, MNRAS, 381, 1018
 Astier, P., Guy, J., Regnault, N., et al. 2006, A&A, 447, 31
 Blake, C. & Glazebrook, K. 2003, ApJ, 594, 665
 Calzetti, D., Armus, L., Bohlin, R. C., et al. 2000, ApJ, 533, 682
 Capak, P., Aussel, H., Ajiki, M., et al. 2007, ApJS, 172, 99
 Coe, D., Benítez, N., Sánchez, S. F., et al. 2006, AJ, 132, 926
 Coleman, G. D., Wu, C.-C., & Weedman, D. W. 1980, ApJS, 43, 393
 Dahlen, T., Mobasher, B., Jouvel, S., et al. 2008, AJ, 136, 1361
 Dahlen, T., Mobasher, B., Somerville, R. S., et al. 2005, ApJ, 631, 126
 Giavalisco, M., Ferguson, H. C., Koekemoer, A. M., et al. 2004, ApJ, 600, L93
 Glazebrook, K. & Blake, C. 2005, ApJ, 631, 1
 Grazian, A., Fontana, A., de Santis, C., et al. 2006, A&A, 449, 951
 Ilbert, O., Arnouts, S., McCracken, H. J., et al. 2006, A&A, 457, 841
 Ilbert, O., Capak, P., Salvato, M., et al. 2009, ApJ, 690, 1236
 Iovino, A., McCracken, H. J., Garilli, B., et al. 2005, A&A, 442, 423
 Jouvel, S., Kneib, J.-P., Bernstein, G., et al. 2009, in prep.
 Kennicutt, Jr., R. C. 1998, ARA&A, 36, 189
 Kilbinger, M., Benabed, K., Guy, J., et al. 2009, A&A, 497, 677
 Koekemoer, A. M., Aussel, H., Calzetti, D., et al. 2007, ApJS, 172, 196
 Lamareille, F., Brinchmann, J., Contini, T., et al. 2008, ArXiv e-prints
 Lawrence, A., Warren, S. J., Almaini, O., et al. 2007, MNRAS, 379, 1599
 Le Fèvre, O., Vettolani, G., Garilli, B., et al. 2005, A&A, 439, 845
 Leauthaud, A., Massey, R., Kneib, J.-P., et al. 2007, ApJS, 172, 219
 Ma, Z. & Bernstein, G. 2008, ApJ, 682, 39
 Madau, P. 1995, ApJ, 441, 18
 Massey, R., Rowe, B., Refregier, A., Bacon, D. J., & Bergé, J. 2007, MNRAS, 380, 229
 McCall, M. L., Rybski, P. M., & Shields, G. A. 1985, ApJS, 57, 1
 McCracken, H. J., Radovich, M., Bertin, E., et al. 2003, A&A, 410, 17
 Mouhcine, M., Lewis, I., Jones, B., et al. 2005, MNRAS, 362, 1143
 Moustakas, J., Kennicutt, Jr., R. C., & Tremonti, C. A. 2006, ApJ, 642, 775
 Perlmutter, S., Aldering, G., Goldhaber, G., et al. 1999, ApJ, 517, 565
 Riess, A. G., Filippenko, A. V., Challis, P., et al. 1998, AJ, 116, 1009
 Sawicki, M. J., Yee, H. K. C., & Lin, H. 1996, JRASC, 90, 337
 Zoubian, J. & Kneib, J.-P. 2009, in prep.